# 國立交通大學

## 電機學院微電子奈米科技產業研發碩士班

## 碩 士 論 文

# 表面處理及上電極金屬對有機場效應電晶體之漏電流分析

# Analyzing the influence of surface treatment and different top electrodes on the leakage current of organic thin-film transistors

研 究 生：呂成家

指導教授：張國明 教授

中 華 民 國 九 十 八 年 十 一 月

# 表 面 處 理 及 上 電 極 金 屬 對 有 機 場 效 應 電 晶 體 之 漏 電 流 分 析

# Analyzing the influence of surface treatment and different top electrodes on the leakage current of organic thin-film transistors

研 究 生：呂成家　　Student：Cheng-Jia Lui

指導教授：張國明　　Advisor：Kow-Ming Chang

國 立 交 通 大 學

電機學院微電子奈米科技產業研發碩士班

碩 士 論 文

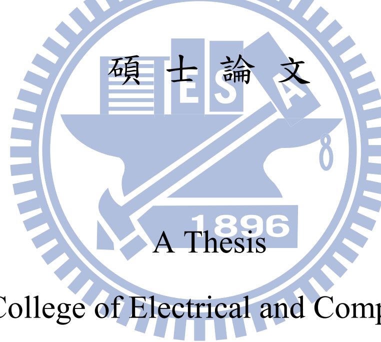


A Thesis

Submitted to College of Electrical and Computer Engineering

National Chiao Tung University

in partial Fulfillment of the Requirements

for the Degree of

Master

in

Industrial Technology R & D Master Program on
Microelectronics and Nano Sciences

October 2009

Hsinchu, Taiwan, Republic of China

中華民國九十八年十一月

# 表面處理及上電極金屬對有機場效應電晶體之漏電流分析

學生：呂成家　　　　　　　　　　　　　指導教授：張國明　博士

國立交通大學電機學院產業研發碩士班

## 摘　　要

有機薄膜電晶體上常見之漏電流對特性曲線造成的扭曲現象在本研究中已被詳細的解釋，閘極感應汲極漏電流將造成元件之輸出曲線於靜態時的漂移，而轉換曲線於靜態時的漂移則由閘極感應汲極漏電流和汲極/源極間靜態漏電流所共同提供。另外絕緣層表面之疏水性處理對漏電流的影響亦被分析，經由對絕緣層表面之處理，可使有機半導體分子層在沉積鍵結的過程趨於完整，但伴隨而來的則是漏電流的增加。最後換置不同功函數之金屬當做汲/源極電極材料，並對金屬和有機物接面之接觸電阻對漏電流影響做一分析，在我們的研究中得出漏電流和接觸電阻有直接關係，但接觸電阻與金屬對有機物解離能之差並無直接關聯性。

# Analyzing the influence of surface treatment and different top electrodes on the leakage current of organic thin-film transistors

Student: Cheng-Jia Lui Advisors: Dr. Kow-Ming Chang

Industrial Technology R & D Master Program of
Electrical and Computer Engineering College
National Chiao Tung University

## ABSTRACT

The origin which caused the distortion of performance curves had been fully analyzed in this thesis. The gate induced drain leakage current will causing the shift in output characteristic curve at off-state. Additionally, the shift in transfer characteristic curves is due to the gate induced drain leakage current and static-state leakage current of source/drain electrode.

Furthermore, the influence of surface hydrophobic treatment on leakage current had been analyzed. After treatment on insulator/semiconductor surface, the order of organic semiconductor will tend to integrity. But the leakage current is the inevitable supplementary impact.

Finally, the material with different work function was used to be the electrode. We analyzed the relationship between the difference of work function and ionization potential (IP) of organic semiconductor, contact resistance, and leakage current. The leakage current had direct correlation with contact resistance, yet to examine the relationship between organic semiconductors and metal is an important work in state-of-the-art OTFTs.

# 誌　謝

本論文得以完成，首先要感謝的是我的指導老師張國明教授，在碩士班兩年期間給予我熱心的指導，使我在這兩年間對於做實驗的態度與了解有相當大的成長，另外也要感謝鄧一中博士及賴瓊惠博士的卓見與指正，使學生的論文更趨於完備，對於老師的諄諄教誨，在此致上我最真摯的感謝。

接著要感謝實驗室的各位學長，同學於我實驗上與生活上的幫助，承蒙黃士軒學長在實驗內容，及論文報告上的幫助，論文口試才得以順利進行，並且要感謝黃菘宏學長、張庭嘉學長、徐明頤學長、洪佑昇同學、賴威仁同學、還有光電所的林建輝同學等等.…於實驗儀器設備的訓練指導，後續的實驗才得以順利進行。

最後要特別感謝黃馨慧同學及其家人在碩士班兩年中生活的陪伴，以及父母親自小的栽培，我才比較沒有後顧之憂的讀書，在此將完成學業之際，僅以此獻給我最摯愛的家人、以及每個關心我的人。

# Contents

Chinese Abstract……………………………..……………………………….i
English Abstract…………………………..…………………………………..ii
Acknowledgement……………………………………………...………...……….iii
Contents…………………………………………………….……………………iv
Table Captions……………………………………………...……….………..vi
Figure Captions……………………………….……………...………………vii
List of symbols…………………………………………………..……....……...x

Chapter 1 Introduction……………………………………………………………1
1.1 Overview of OTFTs technology………………………………………………...1
1.1.1 Operating mode of top contact OTFTs……………………………………..2
1.1.2 Organic semiconductor materials-Poly(3-hexylthiophene)…………………...3
1.1.3 Surface treatment……………………………………………………………...5
1.1.4 Contact resistance in OTFTs……………………..………………………...…….6
1.2 Motivation………………………………………………...…………………6
1.3 Thesis organization……………………………………………………………...7
Chapter 2 Experiment……………………………………………………………...17
2.1 Fabrication of OTFTs……………………………………………………………17
2.2 Transfer length method……………………………...………………...…………19
Chapter 3 Results and discussion……………………………………...………..25
3.1 The influence of leakage current on performance curve…………………...…….25
3.1.1 The adverse impact on output characteristics curve……………………………25
3.1.2 The methods of measurement……………………………………………..27
3.1.3 The examination of difference on leakage current between patterning active layer and without…………………………...………….28
3.2 The influence of surface treatment on leakage current………………...………...29

3.3 The influence of electrode metals on leakage current……………..……………….30
Chapter 4 Conclusion and future work……………………………………………….……58
4.1 Conclusion………………………………………...………………………...58
4.2 Future work…………………………………………...………………………59

References……………………………………………………...……………………….60

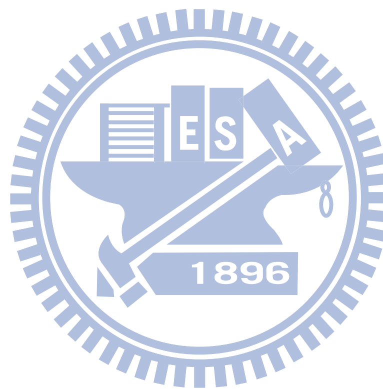

# Table Captions

Table 1-1. Highest field effect mobility(μ) values measured from OTFTs as report in the literature annually from 1986 through 2000…….........................................................................................9

Table 3-1 The parameter of all metals which measured with the transfer length method……...……....57

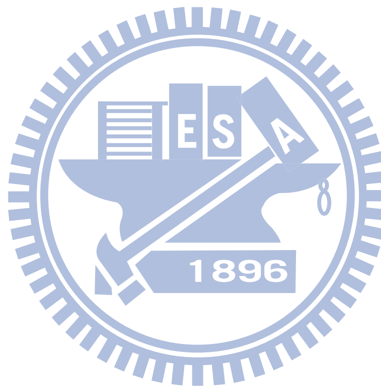

# Figure Captions

Figure 1-1 Semilogrithmic plot of the highest field effect mobility(μ). Report for OTFTs fabricated from the most promising polymeric and oligomeric semiconductors versus year from 1986 to 2000……………………………………………………….…………………………..8

Figure 1-2 The Schema of OTFTs structures consist of (a) bottom contact (BC), and (b) top contact (TC)...........................................................................................................10

Figure 1-3 Schematic of operation of organic thin film transistor, showing a lightly doped semiconductor: "+" indicates a positive charge in semiconductor; "-"indicates a negative charge in semiconductor as (a) no-bias, (b)depletion mode, (c)accumulation mode, (d)non-uniform charge density, (e)pinch-off of channel, (f)and (g)growth of the depletion zone…………………………………………………………..………….…..……..13

Figure 1-4 molecular structure of polyacetylene and energy bands in crystalline molecular solids...........................................................................................................................13

Figure 1-5 The structures of the polymer chain of $P_3HT$………………………..……………………14

Figure 1-6 The different orientations of the HT-$P_3HT$ which consist of (a) spin-coating has the molecules lying flat (face-on) on the silicon wafer and the (b) drop-cast sample has the molecules standing upright (Edge-on)………………..……………………...…….…..14

Figure 1-7 (a) Effect of UV light exposure time on the surface contact angle and the surface energy following ODMS treatment. (b) Schematic shows the chemical bonds modified during UV light exposure. (c) Transfer characteristics of various OTFTs fabricated on ODMS-treated substrate. Conventional devices were OTFTs without any treatment or UV exposure……………………………………………………..………………………..15

Figure 1-8 The output characteristic curves of pentacene TFT with (a) CuO and (b) Cu electrode…...16

Figure 2-1 Effects of pentacene morphology at the contact edge and on source/drain contacts……..…21

Figure 2-2 Fabrication procedure of a actual OTFT of this study……………………………………...22

Figure 2-3 Cross section of the integrated $P_3HT$ FET and MEH-PPV LED. The device is a part (shown inside the dashed area in the top left corner) of a full active-matrix polymer LED pixel. The

lamellar structure of the regioregular $P_3HT$ and its orientation relative to the $SiO_2$ substrate and the direction of the in-plane FET current *I*d is shown schematically…………………23

Figure 2-4 A transfer length method test structure and a plot of total resistance as a function of contact spacing, L………………………………………………………………………..…23

Figure 2-5 Cross-section of an actual test structure of contact resistance in this study……………...…24

Figure 3-1 The performance curves of OTFTs (W/L = 1600/200μm, w/o pattern) as: (a) output characteristic curves, (b) expanded $I_D$-$V_D$ curves, (c) $I_G$-$V_D$ curves, (d) $I_S$ & $I_D$-$V_D$ curves…………………………………………...…………………………….…33

Figure 3-2 The performance curves of OTFTs with the same device as in Fig. 3-1： (a) transfer characteristic curves, (b) $|I_D|$-$V_G$ curves, (c) $I_G$-$V_G$ curves, (d) $I_D$ & $I_S$-$V_G$ curves………....35

Figure 3-3 The curve of $I_{DS\ leakage}$ while gate electrode is floated, and the embedded diagram is leakage current schema……………………………………………………………………..…..36

Figure 3-4 The curves of $I_{G\ leakage}$, and the embedded diagram is gate leakage current schema. As the illustration, due to the uniformity of a transistor on a die, $I_G$ ≒ $2I_D$ ($I_D$ ≒ $I_S$)…...................…36

Figure 3-5 The curves of (a) $I_{D\ leakage}$ and (b) $I_{S\ leakage}$…………………………...……………………...37

Figure 3-6 The performance curves of OTFTs (with pattern) with the same W/L ratio as in Fig. 3-1 as: (a) output characteristic curves, (b) expanded $I_D$-$V_D$ curves, (c) comparing with Fig. 3-1(a), (d) comparison of $I_{D\ leakage}$……………………………………………..……………..…39

Figure 3-7 The curves of (a) $I_G$-$V_D$ (with pattern), (b) comparison of $I_G$-$V_D$, (c) comparison of $I_{G\ leakage}$…………………………………....………..……….….…41

Figure 3-8 The curves of (a) $I_D$ & $I_S$-$V_D$, (b) comparison of $I_S$, (c) comparison of $I_{S\ leakage}$…………..…42

Figure 3-9 The performance curves with the same device as in W/L ratio as in Fig. 3-6 as: (a) transfer characteristic curves, (b) $|I_D|$-$V_G$ curves, (c) comparison of $|I_D|$-$V_G$ curves, (d) $I_G$-$V_G$ curves, (e) comparison of $I_G$-$V_G$ curves, (f) comparison of $I_{DS\ leakage}$…….……………..…45

Figure 3-10 The output characteristic curves of OTFTs which consist of (a) lack of surface treatment, (b) with surface treatment, (c) comparison of (a) and (b), and (d) comparison of $I_{G\ leakage}$……………………………………………………………...…47

Figure 3-11 The transfer characteristic curves of OTFTs which consist of (a) comparison of ID-VG

curves, (b) comparison of |ID|-VG curves, (c) comparison of IDS leakage, (d) comparison of total resistance ($R_T$) versus the length……………………………………………....49

Figure 3-12 The output characteristic curves of OTFTs which consist of (a) Ti electrode, (b) Cr electrode, (c) comparison of $V_G$ = 20V, (d) comparison of $V_G$ = 0V, (e) comparison of $I_{D\ leakage}$……………………………….……………………………..52

Figure 3-13 The transfer characteristic curves of OTFTs which consist of (a) Ti electrode, (b) $|I_D|$-$V_G$ curves of Ti electrode, (c) Cr electrode, (d) $|I_D|$-$V_G$ curves of Cr electrode, (e) comparison of $V_D$ = -20V, (f) comparison of $I_{DS\ leakage}$, (g) comparison of total resistance ($R_T$) versus the length…………………..………………………………………………………...55

Figure 3-14 The curves consist of (a) comparison of total resistance ($R_T$) versus the length and (b) $I_{DS\ leakage}$ with all metals…………………………………...………..………………...…56

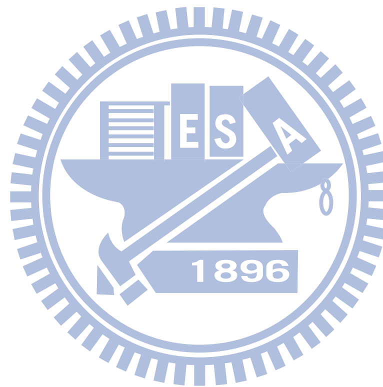

# List of symbols

| Symbol | Description |
|---|---|
| $C_{OX}$ | oxide capacitance /unit area ($F/cm^2$) |
| d | contact length (m) |
| $\Phi_m$ | work function |
| $I_D^*$ | drain current (A) |
| $I_{D\ leakage}$ | leakage current flowing between drain electrode and gate electrode (A) |
| $I_{DS}$ | channel current (A) |
| $I_G$ | gate current (A) |
| $I_{G\ leakage}$ | leakage current flowing between source/drain electrodes and gate electrode (A) |
| $I_S$ | source current (A) |
| $I_{S\ leakage}$ | leakage current flowing between source electrode and gate electrode (A) |
| L | channel length (m) |
| $L_T$ | transfer length (m) |
| $\rho_C$ | specific contact resistivity ($\Omega \cdot cm^2$) |
| $R_C$ | contact resistance ($\Omega$) |
| $R_S$ | sheet resistance ($\Omega/\square$) |
| $R_T$ | total resistance ($\Omega$) |
| $\mu$ | field effect mobility ($cm^2/Vs$) |
| $V_D$ | drain voltage (V) |
| $V_G$ | gate voltage (V) |
| $V_S$ | source voltage (V) |
| $V_{th}$ | threshold voltage (V) |
| W | channel width (m) |

* The positive sign indicates the current flowing into electrode, and negative sign indicates the opposite direction.

# Chapter 1 Introduction

## 1.1 Overview of OTFTs technology

Organic thin film transistors (OTFTs) have become the focus of considerable attention in recent years, because of the wide range of applications in radio-frequency identification (RFID) tags, light-emitting devices, transistors, photovoltaic cells, photodetectors, and flat panel displays etc. Comparing OTFTs with conventional silicon-based transistors, OTFTs are more compatible with polymetric substrates because their advantage in a low-temperature process ( < 180℃). This advantage is not only revealed in the lower thermal but also in the lower cost. Additionally, printing process enable OTFTs advantage of large-area manufacture.

In spite of OTFTs have many advantages, but it has its problems to impede the application in commerce. The relatively low mobility of the organic semiconductors, OTFTs can't rival the performance of FET based on single-crystalline inorganic semiconductors, such as Si, Ge, GaAs, InP, which have charge carrier mobility about three orders of magnitude higher than organic semiconductors. However the performance of OTFT has steadily improved in the last two decades as a result of the development of new organic semiconductors, the optimization of deposition conditions and gate dielectric surface treatments [1]. The semilogarithmic plot of the highest yearly reported field-effect mobility value measured from thin-film transistors based on specific organic semiconductors was presented in Fig1-1, which is based on table1-1 [2].

### 1.1.1 Operating mode of top contact OTFTs

As shown in Fig. 1-2, an OTFT is consisted of three parts as follow: electrodes (gate, source and drain), insulator and organic active layer. Furthermore according to the mutual position of source/drain electrodes and the organic active layer, the transistor can be separated to (a) bottom contact and (b) top contact. We note that BC and TC OTFTs are also commonly referred to as inverted-staggered and inverted-coplanar TFTs, respectively.

The entire operation of transistor is mainly decided according to the on-off state by gate voltage and the current flow through channel by drain voltage. Referring to [3], the operation mode of the $P_3HT$ based OTFTs were operated against to the usual inversion mode of silicon MOSFETs and primarily operated as a P-type accumulation-mode enhancement type transistor. There are four basic modes which will be described late.

Mode 1: When 0V is applied to three electrodes of OTFT. The schematic diagram is shown in Fig. 1-3(a), it is called cut-off. If applied a small drain bias, $V_D$, and the source-current, $I_{DS}$, will be small and ohmic.

Mode 2: When a positive bias applied, the bend bending will occur in the interface between dielectric layer and semiconductor layer. Negative charges will locate at interface and form the depletion region. The schematic diagram is shown in Fig. 1-3(b). The channel resistance is so large that the current will smaller than that of mode 1. Because of the large band gap, inversion layer cannot be observed in the OTFT.

Mode 3: When gate bias is negative, the schematic diagram is shown in Fig. 1-3(c), the voltage is dropped over the insulator and over the semiconductor near the interface between dielectric layer and semiconductor layer. More positive charges will be accumulated in the accumulate region. When a small bias is applied to drain, the source-drain current will be larger than that of Mode 1, and it is called the linear regime which is approximately determined by the following equation:

$$I_{D(lin)} = \frac{W \mu C_{ox}}{2L}[2(V_G - V_{th})V_D - V_D^{\,2}] \qquad (1\text{-}1)$$

where L is the channel length, W is the channel width, $C_{OX}$ is the capacitance per unit area of the insulator layer, $V_{th}$ is the threshold voltage, and $\mu$ is the field effect mobility, which can

be calculated in the linear regime from the transconductance:

$$G_m = \frac{dI_D}{dV_G} = \frac{W}{L}\mu C_{ox} V_D \tag{1-2}$$

by plotting $I_D$ versus $V_G$ at a constant low $V_D$, with $-V_D << -(V_G-V_{th})$, and equating the value of the slope of this plot to $G_m$, then find $G_{m,max}$ which can gain the value of threshold voltage ($V_{th}$) and linear mobility. Finally, the schematic diagram is shown in Fig. 1-3(d).

Mode 4: When drain voltage is negative enough that the voltage difference of gate and drain, $V_{GD}$, which is lower than $V_{th}(<0)$, therefore, the depletion region will form near drain and pitch-off. This kinds of mode is usually called the saturation regime as can been seem in Fig. 1-3(e), and has its approximate equation.

$$I_{D(sat)} = \frac{W\mu C_{ox}}{2L}(V_G - V_{th})^2 \tag{1-3}$$

Similarly, plotting $\sqrt{I_D}$ versus $V_G$ with transfer characteristics curve at a constant high $V_D$, saturation mobility can be extracted. Serially, if drain voltage is more negative, the depletion region would grow and approach source. The schematic diagram is shown in Fig. 1-3 (f) and (g).

## 1.1.2 Organic semiconductor materials–Poly(3-hexylthiophene)

The electrical properties of any material are determined by its electronic structure. The theory that most reasonably explains the material is band theory. In the solid state, the electron orbits of each electron overlap with the same orbits of their neighboring atoms in all directions to produce molecular orbits similar to these in small molecules. When these so many orbits are spaced together in a given range of energies, they form what looks like continuous energy bands. How many electrons these bands are composed of depends on how many electrons the original atomic orbits contain and the energies of the orbits. The highest occupied molecular orbital (HOMO) band is called the valence band, and the lowest unoccupied molecular orbit (LUMO) band is called the conduction band. The energy spacing between the highest occupied band and the lowest unoccupied band is called the band gap ($E_g$).

As can be seen, in Fig. 1-4 polyacetylene is the simplest conjugated polymer and for this reason can be considered as a prototype of other poly conjugated system. Polyacetylene can exist in two isomeric forms: cis-form and trans-form, commonly called cis- and trans-polyacetylene, respectively. The latter form being thermo-dynamically stable since cis-trans isomerization is irreversible. In polyacetylene each carbon atom is $sp^2$ hybridized and for this reason this polymer can be formally treated as one-dimensional analogue of graphite. There exists however an important difference between the bonding system in the graphene plane of graphite and in the polyacetylene chain. Contrary to the case of graphite, the C-C bonds in polyacetylene are not equivalent, i.e. they are alternatively slightly longer and slightly shorter. This is due to so-called Peierls distortion. The described bond non-equivalence has an important effect on electronic properties of polyacetylene because it opens a gap between the HOMO level corresponding to fully occupied π-band (valence band) and the LUMO level corresponding to empty π*-band (conducting band). Thus, in the simplest approach, polyacetylene can be treated as an intrinsic semiconductor with a band gap of 1.5 eV [4].

The field-effect mobility of Poly(3-hexylthiophene), $P_3HT$ is strongly influenced by the structure of the polymer chain and the direction of intermolecular $\pi$ - $\pi$ stacking. The structure of the polymer chain of $P_3HT$ is shown in Fig. 1-5. The 3-alkylsubstituents can be incorporated into a polymer chain with two different regioregularities: head to tail (HT) and head to head (HH).

R represents the alkyl side chain ($C_6H_{13}$ for $P_3HT$), which allows $P_3HT$ to be dissolved in 1 like chloroform. This solution processability enables simple film deposition. A regiorandom $P_3HT$ consists of both HH and HT 3-hexylthiophene in a random pattern while a regioregular has only one kind of 3-hexylthiophene, either HH and HT. This type of order is known as regioregularity and has been shown to give much higher field-effect mobility values over regiorandom material. After being deposited on the substrate, $P_3HT$ backbones may form two different morphologies, edge-on or face-on of lamella structure as shown in Fig. 1-6. The higher mobility is given by edge-on structure since the carriers can move more efficiently

through intra-chain transport along the direction of $\pi$ - $\pi$ stacking.

### 1.1.3 Surface treatment

The interface between an organic material and dielectric layer is a critical factor for device performance. This is because the surface of the dielectric strongly influences the quality of the dielectric/ channel interface and the crystalline organic channel. The quality of interface and the organic channel, as well as the electrical properties of the gate dielectric itself, play a major role in determining the device performance of an OTFT [5-8]. Although several methods have been recently proposed to improve the condition of the interface states, only a few have been proved to be reliable and robust. One of the proposed methods is the use of a self-assembly monolayer (SAM), such as octadecyltrichlorosilane (OTS) [9] and hexamethyldisilazane (HMDS) [10], have been extensively studied. A dielectric surface treatment with OTS is found to improve the mobility of OTFTs.

Another dielectric surface treatment technique is $O_2$ plasma cleaning and subsequent HMDS deposition on dielectrics [10]. A problem owing to $O_2$ plasma cleaning, which is applied to remove residues generated from previous photolithography processes, was found to be the generation of a large number of trap states during the cleaning process by assisting OH termination at the $SiO_2$ surface [11]. Although a HMDS layer subsequently applied is expected to reduce the number of traps and act as a SAM, the time-consuming wet processes used to apply a SAM on the interface are unreliable and can cause other undesirable contaminations of the device.

Surface treatments using an ion beam have been widely studied in other research fields. It is well known that ion implantation techniques can change the surface conditions or thin-film properties [12]. In the LCD fabrication process, for example, Ar ion beam treatment has been considered as a viable option as a surface treatment method to replace conventional contact-based treatment such as rubbing [13]. One of the advantages of Ar ion beam treatment is that because argon is an inert gas, it can clean the surface effectively without affecting the chemical structure of the dielectric layer.

### 1.1.4 Contact resistance in OTFTs

There are many parameter will impact the characteristics of OTFTs. The contact resistance between the source/drain electrodes and the organic semiconductor is an important problem. This is because the current of device was so low that the performance would mainly be limited by contact resistance after the mobility of organic semiconductor was improved [14].

Material of source/drain electrodes and the structure both affect the contact characteristics between the source/drain electrode and the organic semiconductors. Unlike the FET of single-crystalline silicon, polycrystalline silicon, or hydrogenated amorphous silicon, the $P_3HT$ material cannot be optimized easily by semiconductor doping or silicide formation. Such properties of organic semiconductors deteriorate the performance of devices; moreover, the chemical compound always increase the contact resistance between the source/drain electrode and the organic semiconductor [15]. It is a straightforward method to find a suitable electrode material which forms ohmic contact with the organic active layer and thus to improve the performance of OTFTs. In general, many researcher believe $P_3HT$ can form an ohmic contact with material for its work function larger than 4.5eV because the work function of $P_3HT$ is 4.5eV. Work functions of all materials we used are larger than 4.5eV; they include Ni(5.15eV), Pd(5.12eV), and Cr(4.5eV).

## 1.2 Motivation

In the progress of OTFTs technology, the surface treatment and the modification of electrode metals had critical influence on performance. However, while the researcher concentrated on the performance of device, the fundamental theorem and the usual phenomenon is needed to clarify in the territory of OTFTs.

As shown in Fig.1-7 (a) [16], the author proposed the pentacene-based OTFTs grown on a self-assembled monolayer (SAM)-treated dielectric with various functional groups and molecular lengths, and proceed with the exposure to ultra violet (UV) light. And over time, the chemical bonds of ODMS such as C-C, C-H, and C-Si were decomposed by UV light as

the illustration in Fig.1-7 (b). Consequently, the contact angle was altered when the chemical bonds were excited to form polar functional groups (e.g., CHO, COOH etc.). The decomposed ODMS on the $SiO_2$ surface made the surface hydrophilic and increased the surface energy. Finally, the dendritic-like grain and the disordered pentacene crystal phase lead to the decrease of on-current as in Fig. 1-7(c). However, just like the part which many papers lacked for mention is the distortion phenomenon at the off-state (When $V_G$ approach 0V).

Additionally, Fig. 1-8 is related to modification of electrode [17]. The author proposed a material of higher work function to obtain a higher on-current as illustration in Fig. 1-8(a). But comparing to Fig. 1-8(b), the shift phenomenon at off-state (When $V_D$ approach 0V) is more serious. The origin which cause the distortion of performance curves were not mentioned, too.

Whereas the usual phenomenon which lack for clarification in the territory of OTFTs, we wrote a study of leakage phenomenon at different modifications

## 1.3 Thesis organization

This thesis is organized as follow：

In Chapter 1, the background of OTFTs and the motivation of our study were described.

In Chapter 2, the fabrication procedure of the transistor was described. Additionally, the transfer length method (It is also abbreviated as TLM.) was adopted to measure the contact resistance, and the relative theorem was described, too.

In Chapter 3, the influence of leakage current on output and transfer characteristics curve was observed. Furthermore, the leakage current of OTFTs which fabricated with and without a hydrophobic treatment of gate insulator was analyzed. In general, most researches only indicated the advantages of the surface treatment on gate insulator and they did not point out the influence of it on leakage current. On the other hand, various electrode metals were employed to obtain the relation with leakage current which is also to examine in this chapter.

In Chapter4, conclusions as well as some recommendations for further study are given.

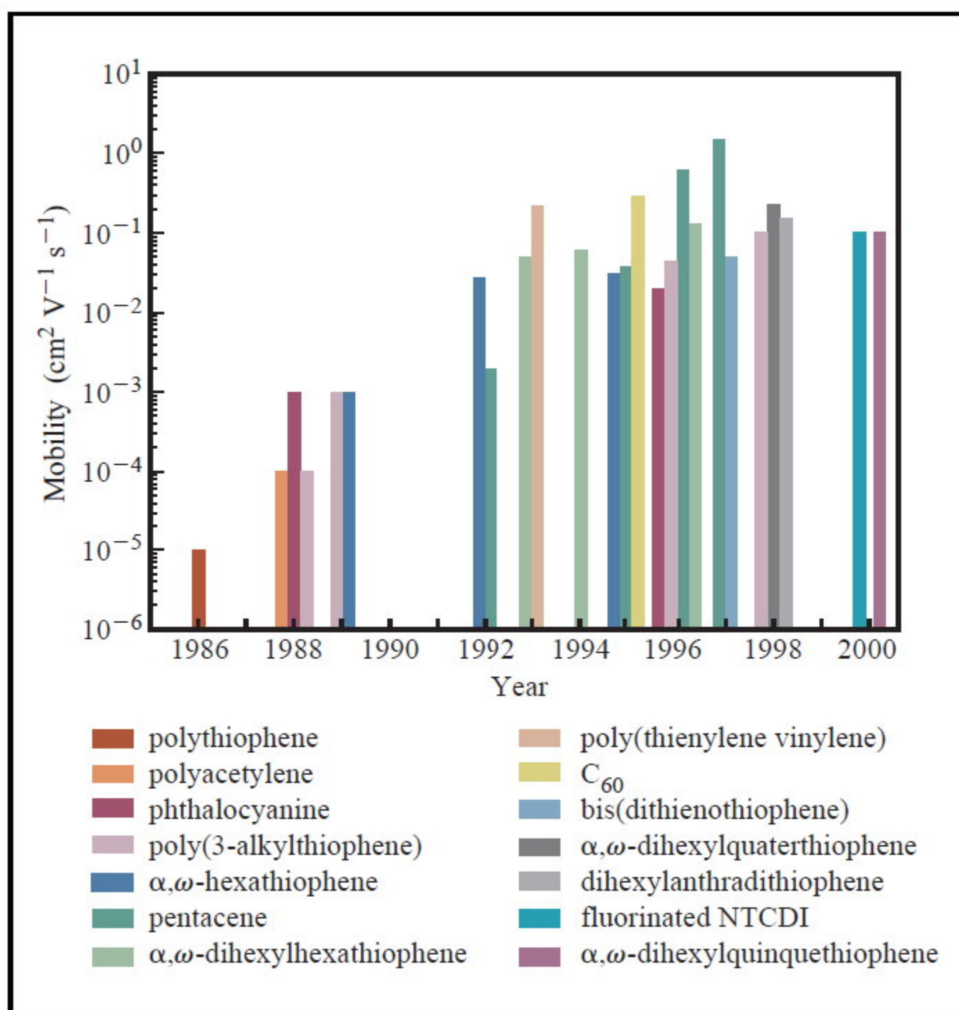


Figure 1-1. Semilogrithmic plot of the highest field effect mobility( $\mu$ ). Report for OTFTs fabricated from the most promising polymeric and oligomeric semiconductors versus year from 1986 to 2000[2].

Table 1-1. Highest field effect mobility( $\mu$ ) values measured from OTFTs as report in the literature annually from 1986 through 2000[2].

| *Year* | *Mobility* ($cm^2\ V^{-1}\ s^{-1}$) | *Material (deposition method)* (v) = vacuum deposition (s) = from solution | $I_{on}/I_{off}$* | *W/L* | *Reference* |
|---|---|---|---|---|---|
| 1983 | Minimal, not reported (NR) | Polyacetylene (s) (demonstration of field effect in an OTFT) | NR | 200 | [16] |
| 1986 | $10^{-5}$ | Polythiophene (s) | $10^3$ | NR | [17] |
| 1988 | $10^{-4}$ | Polyacetylene (s) | $10^5$ | 750 | [18] |
| | $10^{-3}$ | Phthalocyanine (v) | NR | 3 | [19] |
| | $10^{-4}$ | Poly(3-hexylthiophene) (s) | NR | NR | [20] |
| 1989 | $10^{-3}$ | Poly(3-alkylthiophene) (s) | NR | NR | [21] |
| | $10^{-3}$ | α–ω-hexathiophene (v) | NR | NR | [22] |
| 1992 | 0.027 | α–ω-hexathiophene (v) | NR | 100 | [23] |
| | $2 \times 10^{-3}$ | Pentacene (v) | NR | NR | ibid. |
| 1993 | 0.05 | α–ω-di-hexyl-hexathiophene (v) | NR | 100–200 | [24] |
| | 0.22† | Polythienylenevinylene (s) | NR | 1000 | [25] |
| 1994 | 0.06 | α–ω-dihexyl-hexathiophene (v) | NR | 50 | [26] |
| 1995 | 0.03 | α–ω-hexathiophene (v) | $>10^6$ | 21 | [27] |
| | 0.038 | Pentacene (v) | 140 | 1000 | [28] |
| | 0.3 | $C_{60}$ (v) | NR | 25 | [29] |
| 1996 | 0.02 | Phthalocyanine (v) | $2 \times 10^5$ | NR | [30] |
| | 0.045 | Poly(3-hexylthiophene) (s) | 340 | 20.8 | [31] |
| | 0.13 | α–ω-dihexyl-hexathiophene (v) | $>10^4$ | 7.3 | [15] |
| | 0.62 | Pentacene (v) | $10^8$ | 11 | [32] |
| 1997 | 1.5 | Pentacene (v) | $10^8$ | 2.5 | [33] |
| | 0.05 | Bis(dithienothiophene) (v) | $10^8$ | 500 | [34] |
| 1998 | 0.1 | Poly(3-hexylthiophene) (s) | $>10^6$ | 20 | [35] |
| | 0.23 | α–ω-dihexyl-quaterthiophene (v) | NR | 1.5 | [36] |
| | 0.15 | Dihexyl-anthradithiophene | NR | 1.5 | [37] |
| 2000 | 0.1 | n-decapentafluoroheptyl-methyl-naphthalene-1,4,5,8-tetracarboxylic diimide (v) | $10^5$ | 1.5 | [38] |
| | 0.1 | α–ω-dihexyl-quinquethiophene (s) | NR | NR | [38] |

*Values for $I_{on}/I_{off}$ correspond to different gate voltage ranges and thus are not readily comparable to one another. The reader is encouraged to read the details of the experiments in the cited references.

†This result has not yet been reproduced.

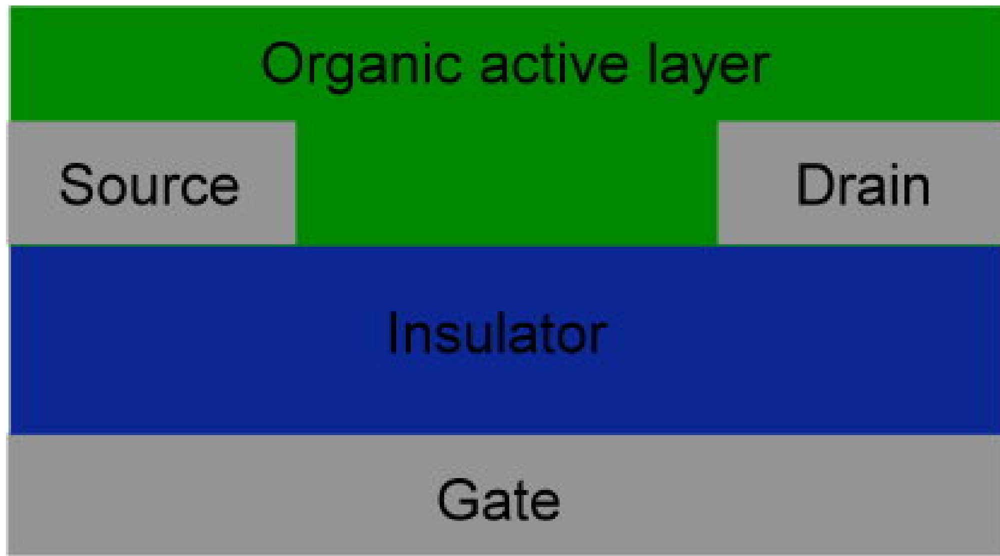


(a)

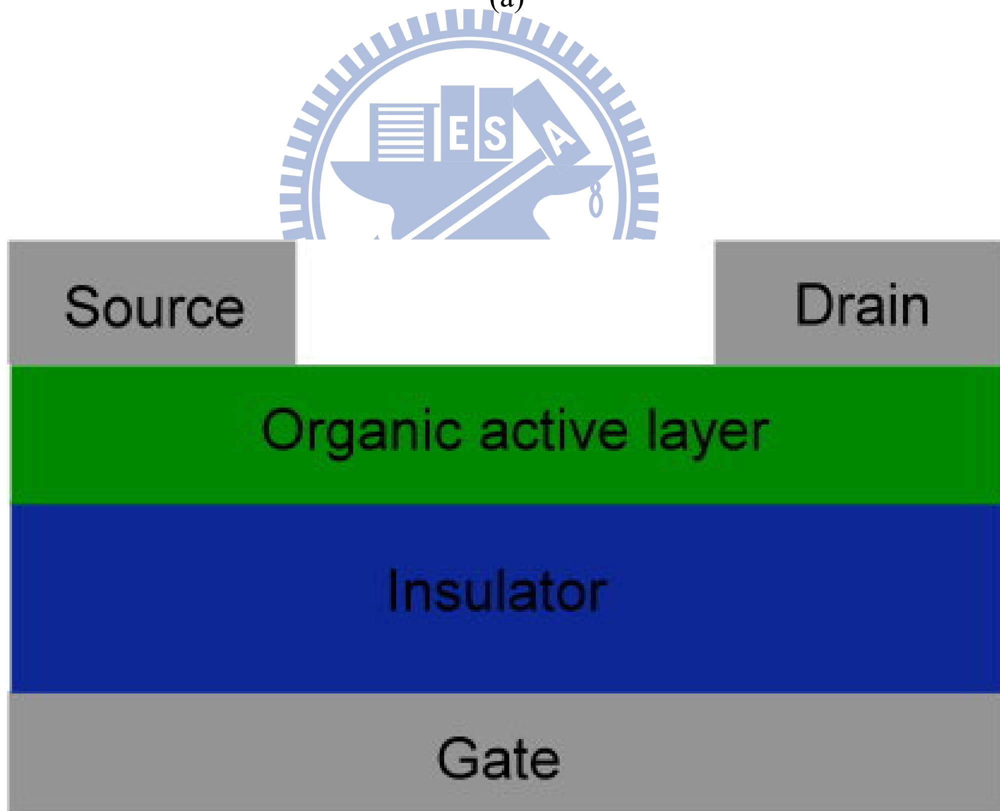


(b)

Figure 1-2. The schema of OTFTs structures consist of (a) bottom contact (BC), and (b) top contact (TC).

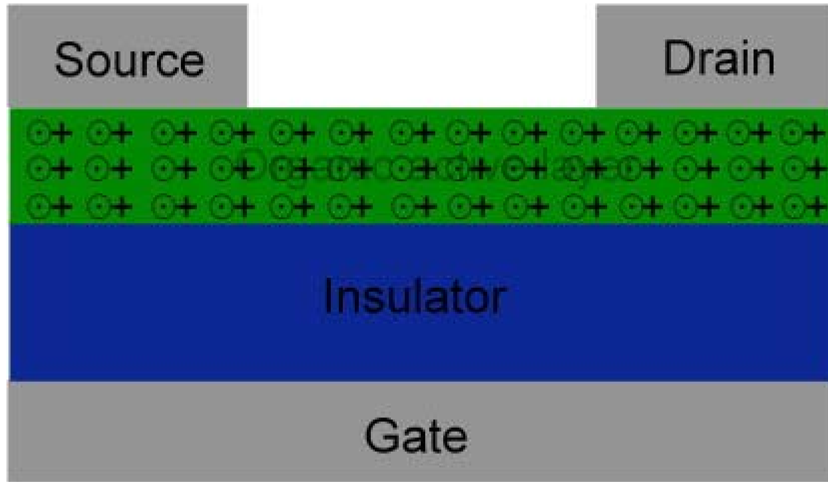


(a) $V_G=V_S=V_D=0$

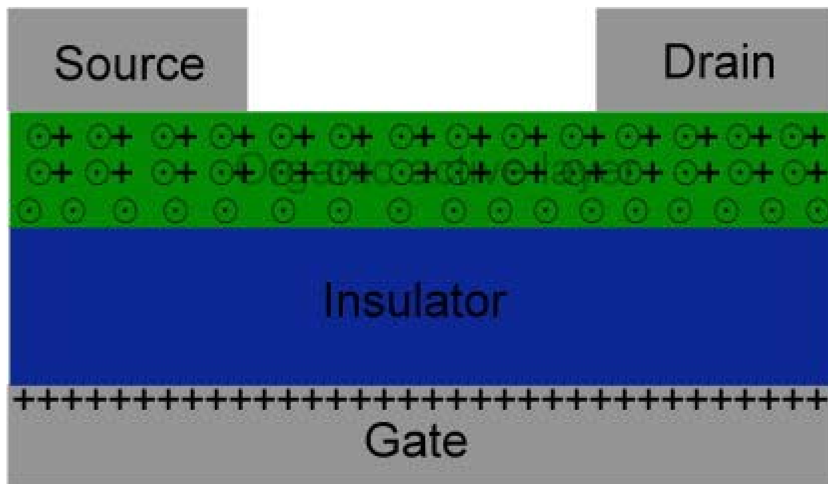


(b) $V_S=V_D=0$ , $V_G > 0$

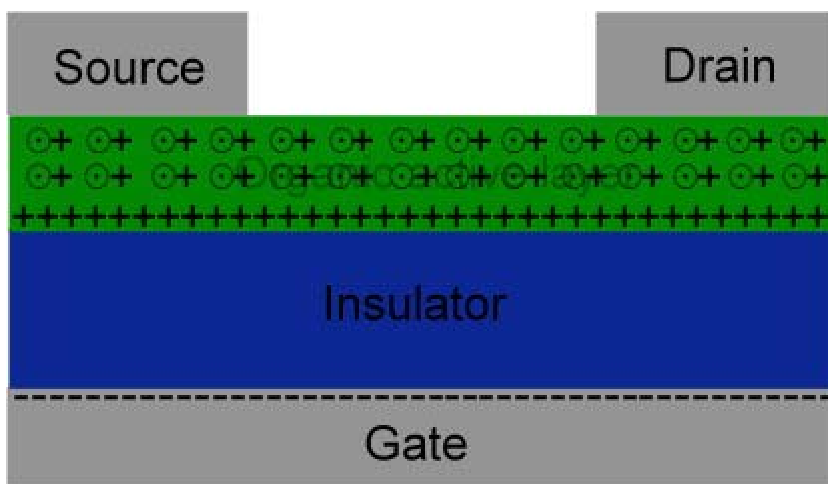


(c) $V_S=V_D=0$, $V_G < 0$

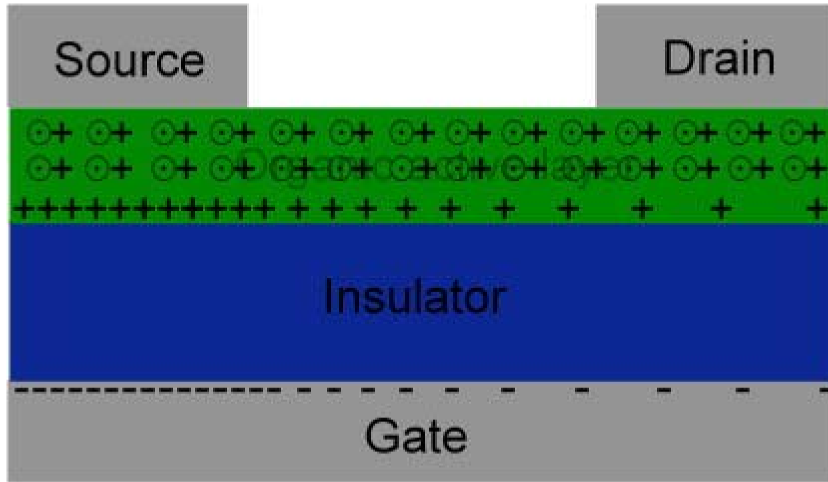


(d) $V_S=0, V_G < V_D < 0$

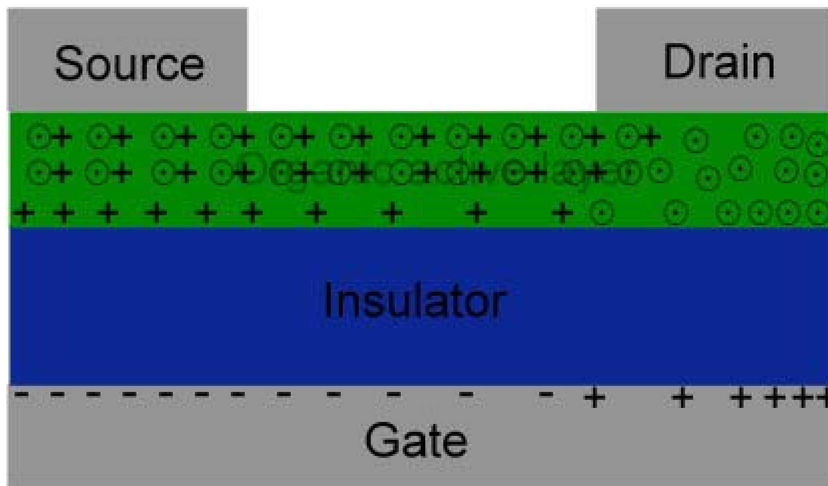


(e) $V_S=0, V_D < V_G < 0$

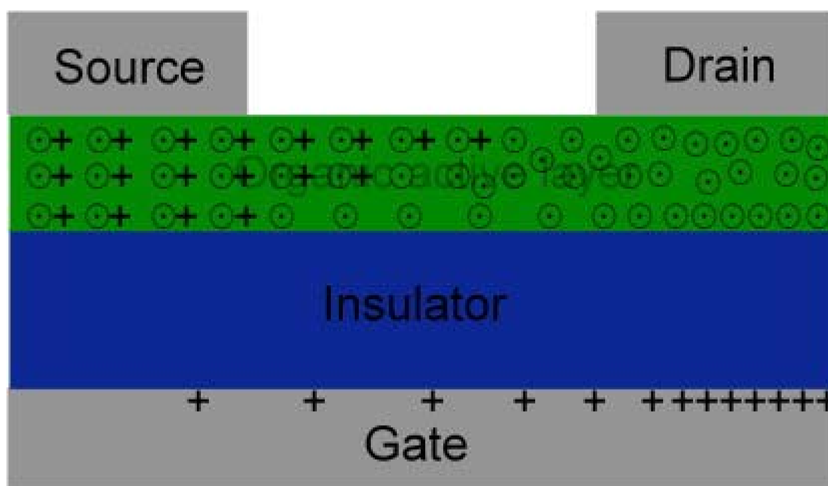


(f) $V_S= V_G=0, V_D < 0$

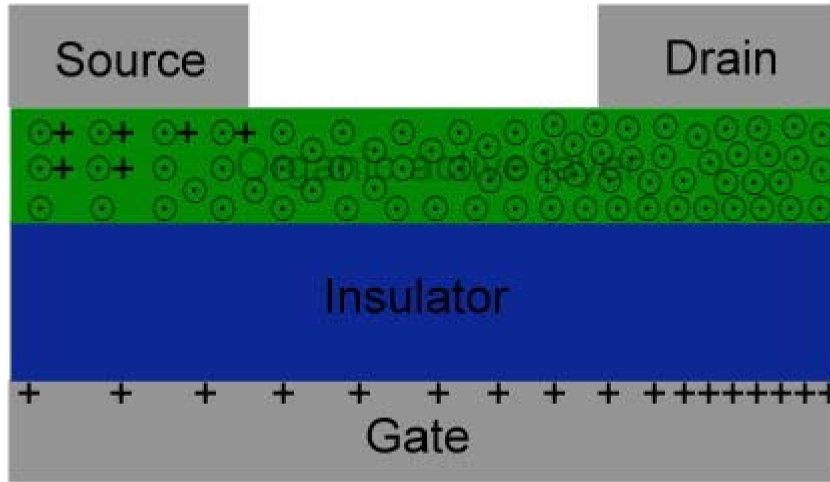


(g) $V_S = V_G = 0$, $V_D << 0$

Figure 1-3. Schematic of operation of organic thin film transistor, showing a lightly doped semiconductor: "+" indicates a positive charge in semiconductor; "-"indicates a negative charge in semiconductor as (a) cut-off mode, (b)depletion mode, (c)accumulation mode, (d)non-uniform charge density, (e)pinch-off of channel, (f)and (g)growth of the depletion zone.

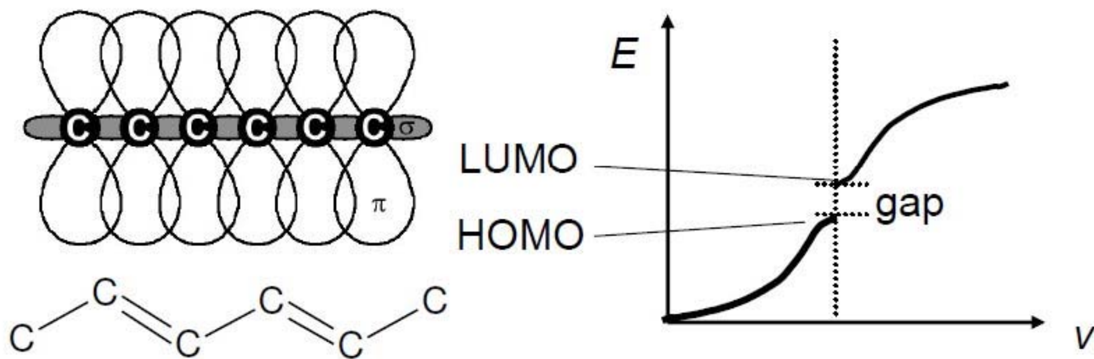


Figure 1-4. molecular structure of polyacetylene and energy bands in crystalline molecular solids.

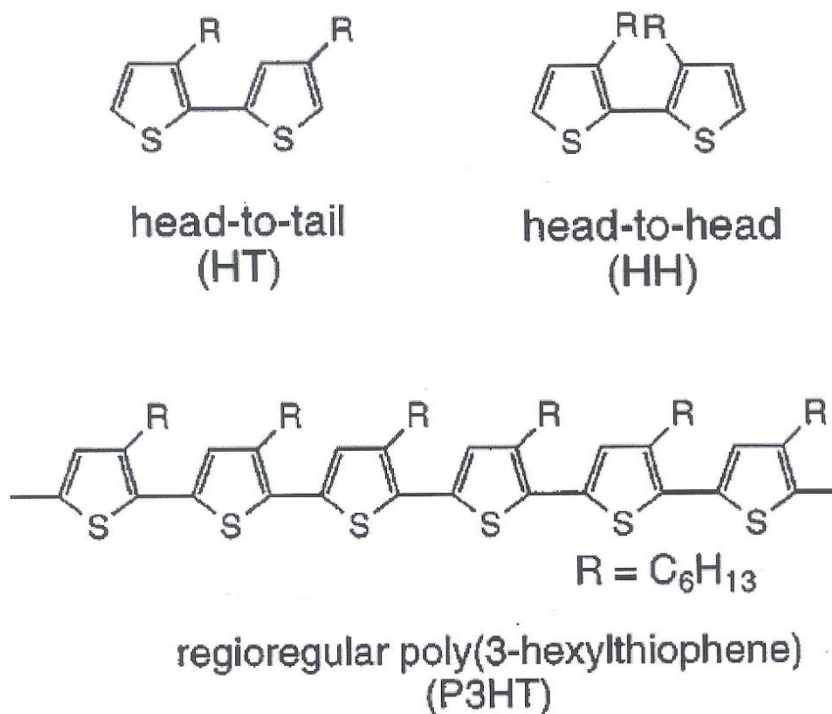


Figure 1-5. The structures of the polymer chain of $P_3HT$.

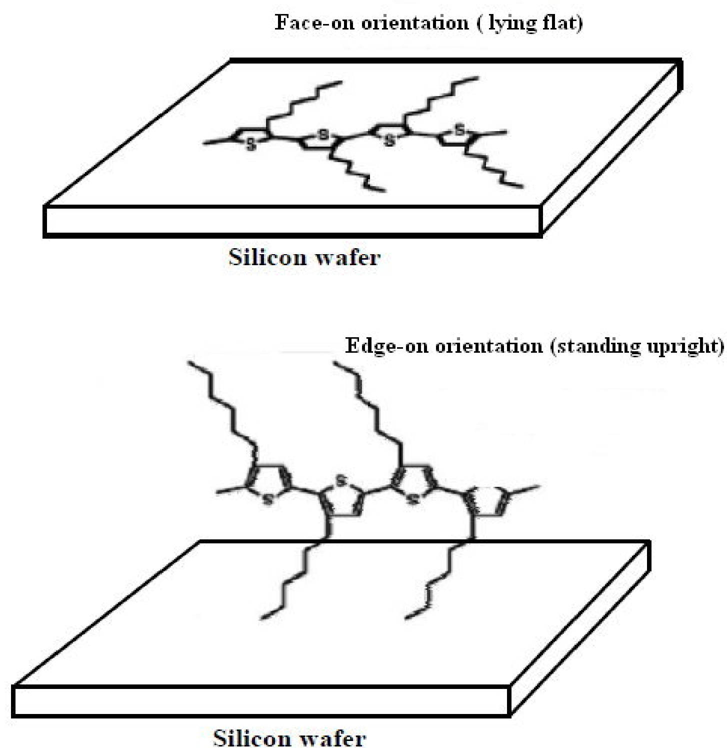


Figure 1-6. The different orientations of the HT-$P_3HT$ which consist of (a) spin-coating has the molecules lying flat (face-on) on the silicon wafer and the (b) drop-cast sample has the molecules standing upright (Edge-on).

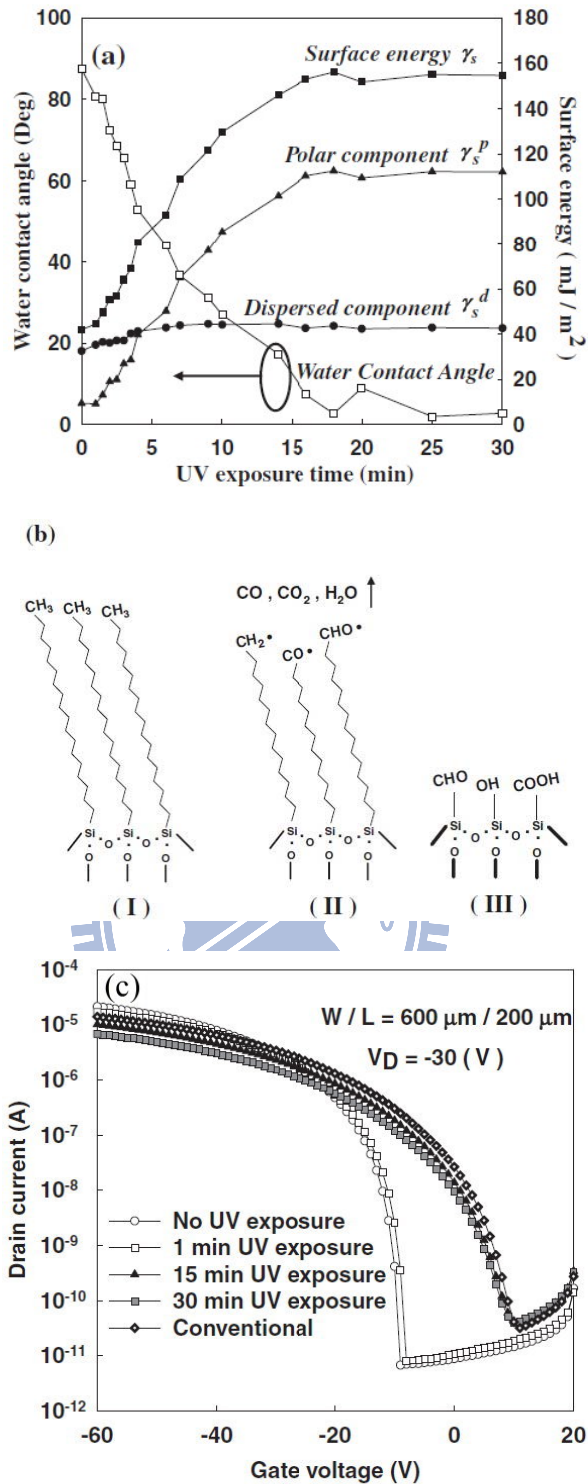


Figure 1-7. (a) Effect of UV light exposure time on the surface contact angle and the surface energy following ODMS treatment. (b) Schematic shows the chemical bonds modified during UV light exposure. (c) Transfer characteristics of various OTFTs fabricated on ODMS-treated substrate. Conventional devices were OTFTs without any treatment or UV exposure [15].

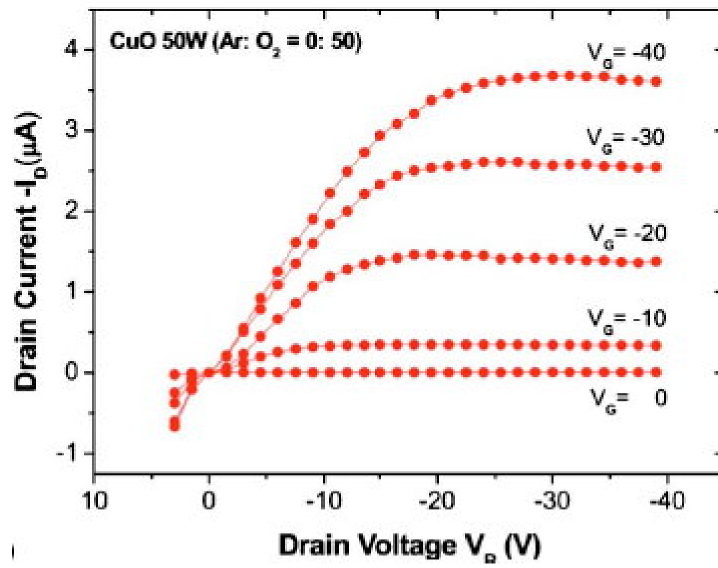


(a)

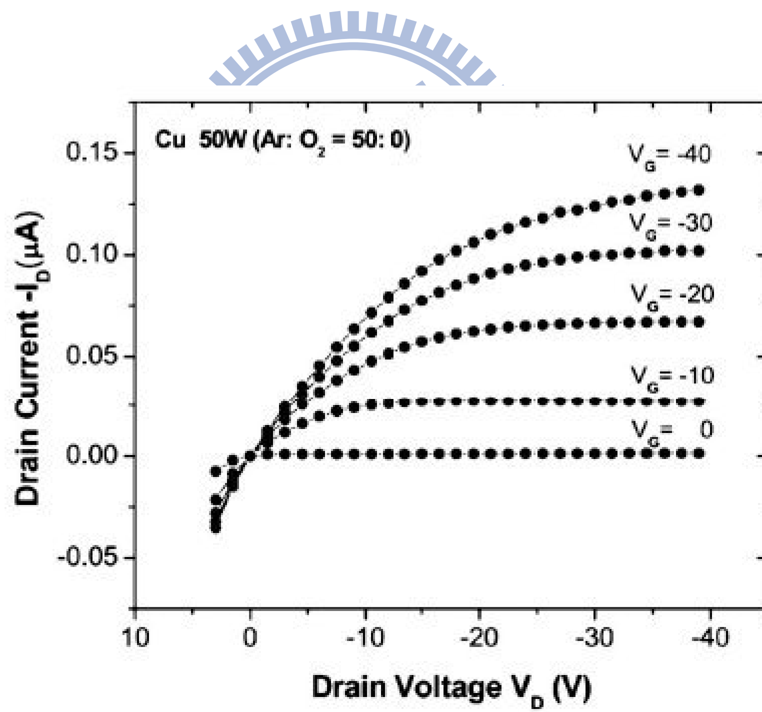


(b)

Figure 1-8. The output characteristic curves of pentacene TFT with (a) CuO and (b) Cu electrode [16].

# Chapter 2 Experiment

## 2.1 Fabrication of OTFTs

Mention in preceding chapter, OTFTs can be distributed into two parts of structure. However, the performance of OTFTs in a bottom contact device structure is generally observed to be inferior to the top contact device configuration [18]. The reason for this difference is often explained by the large metal-semiconductor contact resistance due to interface contact barrier [19] and irregular deposition or poor morphology of the semiconductor film around the already patterned source and drain contacts [20]. Additionally, Dipti Gupta et al. (2009) showed that the pentacene film near the source/drain contact edges exhibits lower mobility region in bottom contact structure [21]. The lower mobility region is due to two kinds of causes.

The first, it is possible that a shadow cast by metal during evaporation of pentacene could lead to unfilled corners at the source/drain contacts, which in turn could result in lower effective device mobility.

The second, when pentacene is deposited on a metal surface, the back bone of the pentacene molecule is attracted to the metal leading to a lying down configuration of pentacene molecules, as illustrate at Fig. 2-1 (e). While on $SiO_2$, low surface energy causes the pentacene molecules to stand vertically, as illustrate at Fig. 2-1 (d). Near the source/drain contact edges, pentacene molecules tend to have both lying down and standing mode leading to poor packing and poor molecular ordering, as illustrate at Fig. 2-1 (c). In this respect, Dipti Gupta et al. also simulated the low-mobility-region for a bottom contact configuration, as illustrate at Fig. 2-1(f) which the width of this low-mobility-region on the insulator is 1μm was determined from Fig. 2-1(a). As can be seen in Fig. 2-1 (g), the introducing of low-mobility-region in the bottom contact devices yields a good comparison with the measured data.

On the basis of above, the low-mobility-region incurs most of potential drop due to which

the extracted mobility from the bottom contact devices becomes significantly lower than the top contact devices, and it is also the source of tumultuous leakage. Therefore to avoid the poor morphology of the semiconductor film around the already patterned source and drain contacts perturbed our measurement, we selected top contact structure to be our device structure of experiment.

The choice of solvents and polymers has a very significant impact on the electrical characteristics of OTFTs. In a recent publication, Bao et al. [22] observed that when chloroform was used as a solvent to make $P_3HT$-base transistors, the field-effect mobility was 0.1cm2$Vs^{-1}$, whereas Tetra hydrofuran (THF) was used as the solvent, the value is noly 6E-4 $cm^2Vs^{-1}$. The performances are influenced by the different solvents of $P_3HT$ with different process conditions [22]. In spite of chloroform is mainly used in solvent of $P_3HT$, however it is toxic to the neural system and its usage is restricted or prohibited in some countries, xylene becomes an appropriate choice deposite its low mobility and solubility to $P_3HT$.

Finally, in the last paragraph of this section, the fabrication procedure will be described as detail. After referred to the papers which contain the spin-on $P_3HT$ thin film transistor [23], we decided the optimize recipes in the fabrication procedure. At first, a n-type bare silicon wafer($\rho$ = 1~10Ω ‧cm) that was used as the substrate and gate electrode was cleaned by the standard RCA clean, and the thermally grown $SiO_2$(dry oxidation at 950℃) provided a high quality gate insulator about thickness 30~40nm which measured with n & k system. Then, these samples are separated into two parts. One was treated with trimethyl(phenyl)silane by atmospheric pressure plasma, and the other did not have. Following surface treatment, an active $P_3HT$ layer was spin-coated at 1500 rpm with and without pattern for 35s and baked on a hot plate at 130℃ for 3min. The $P_3HT$ (with more than 98.5 % head-to-tail linkage) and highly pure solvent (xylene) were obtained from the Aldrich Chemical Company. Solutions of $P_3HT$ in xylene were made with a weight concentration of 0.3 %, and filtered through a 0.45 μm pore PTFE filter. Finally, the source and drain electrodes which used different kinds of metals were deposited by E-gun apparatus. All the process follow is shown in Fig. 2-2.

## 2.2 Transfer length method

To characterize the contact resistance has many methods e.g., the transfer length method (TLM), cross bridge Kelvin resistance (CBKR), and contact end resistance (CER) etc. However, Slimane Oussalah et al. showed that only the transfer length method (TLM) test structure is able to give correct values of the specific contact resistance for both n and p type diffused layers that are compatibles with the manufacturer specifications [24]. It is for this reason why the TLM was employed as the test structure to measure contact resistance in this thesis.

As can be seen in Fig. 2-4 [25], the total resistance is measured for various contact spacing plotted versus L, and two parameters can be extracted from the following equation :

$$R_T = \frac{R_s}{W} L + 2R_C \tag{2-1}$$

where $R_T$ is the total resistance between any two contacts, $R_S$ the sheet resistance, and $R_C$ the contact resistance assumed to be identical for each contacts. The slop $\triangle(R_T)/\triangle(L) = R_S/W$ leads to the sheet resistance with the contact width W independently measured. The intercept at L = 0 is $R_T = 2R_C$ giving the contact resistance.

For contacts with $d \geqq 1.5L_T$, and we use the approximation leading from [26]:

$$R_C = \frac{\rho_C}{L_T W} \coth(d / L_T) \tag{2-2}$$

to

$$R_C \approx \frac{\rho_C}{L_T W} \quad (\text{ for } d > 1.5L_T, \coth(d/L_T) \fallingdotseq 1 ) \tag{2-3}$$

where $\rho_c$ is the specific contact resistivity, and $L_T$ the transfer length is defined as follow:

$$L_T = \sqrt{\rho_C / R_S} \tag{2-4}$$

The total resistance equation as shown in Eq.(2-1) can be rewritten as:

$$R_T = \frac{R_s}{W}(L + 2L_T) \tag{2-5}$$

Therefore, the third parameter can be extracted at the intercept at $R_T = 0$ give $-L = 2L_T$, which leads to the specific contact resistivity with $R_S$ known from the slope of the plot. The transfer

length method gives a complete characteristics of the contact by providing the sheet resistance, the contact resistance, and the specific contact resistivity.

Although the transfer length method is commonly used, but is has its own assumption that must to be satisfied. The $R_S$ must identical under the contacts and between contacts, than the intercept at $R_T = 0$ giving $L_T$ could be distinct, leading to correct $\rho_c$ value.

As can be seen in Fig.2-5, seven identical contacts were deposited on the $P_3HT$ film. The varied kinds of metals were used to examine the relation with contact resistance.

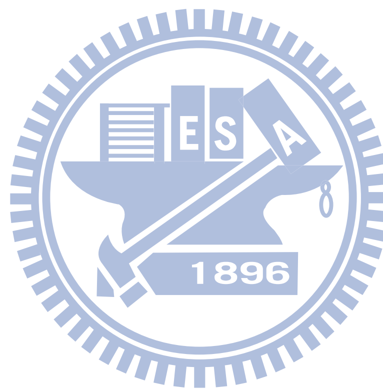

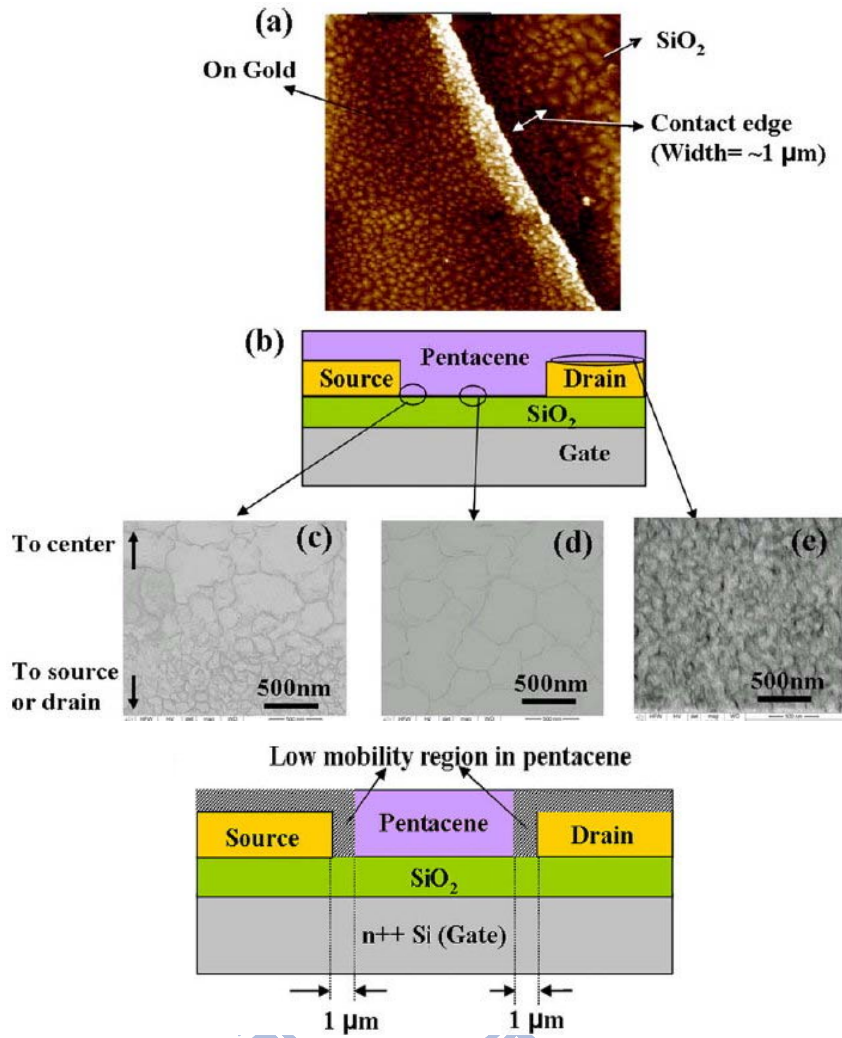


(f) Schema of the 1μm wide low-mobility-region near the source and drain contact edges and above the contacts in bottom contact devices.

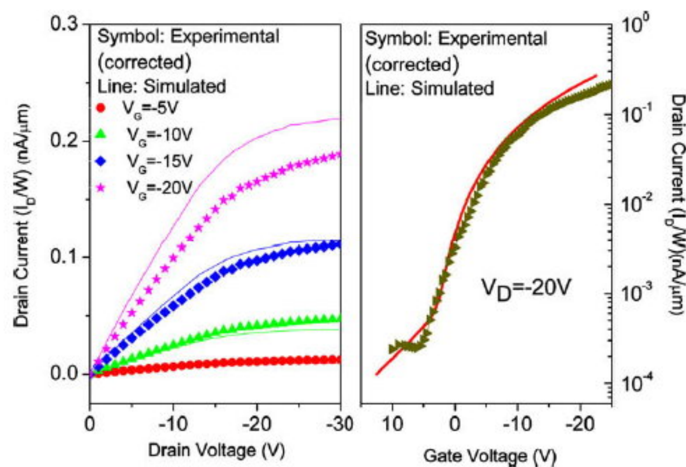


(g) Comparison of the experimental and the simulated curve.

Figure 2-1 Effects of pentacene morphology at the contact edge and on source/drain contacts.

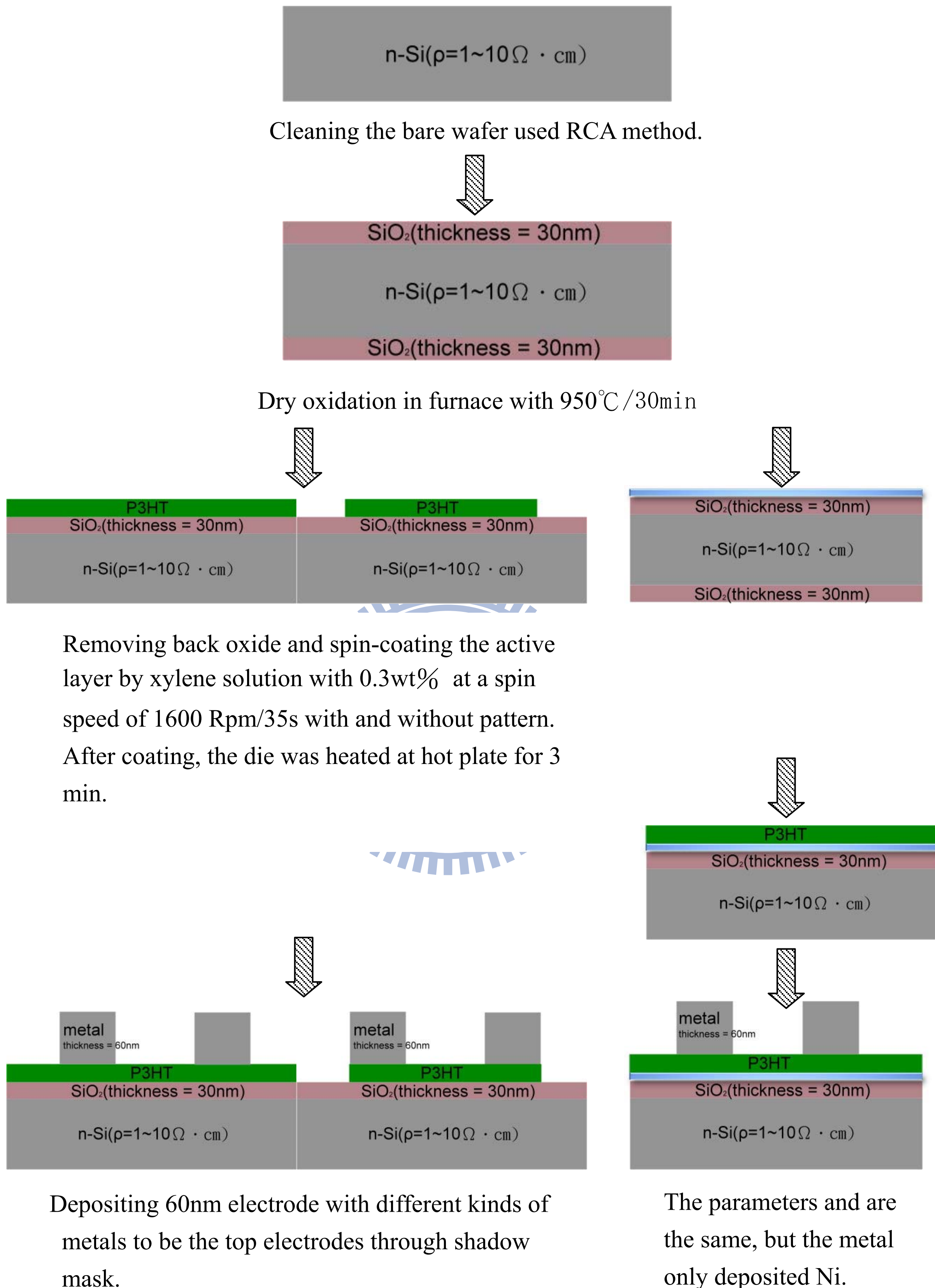


Figure 2-2 Fabrication procedure of a actual OTFT of this study.

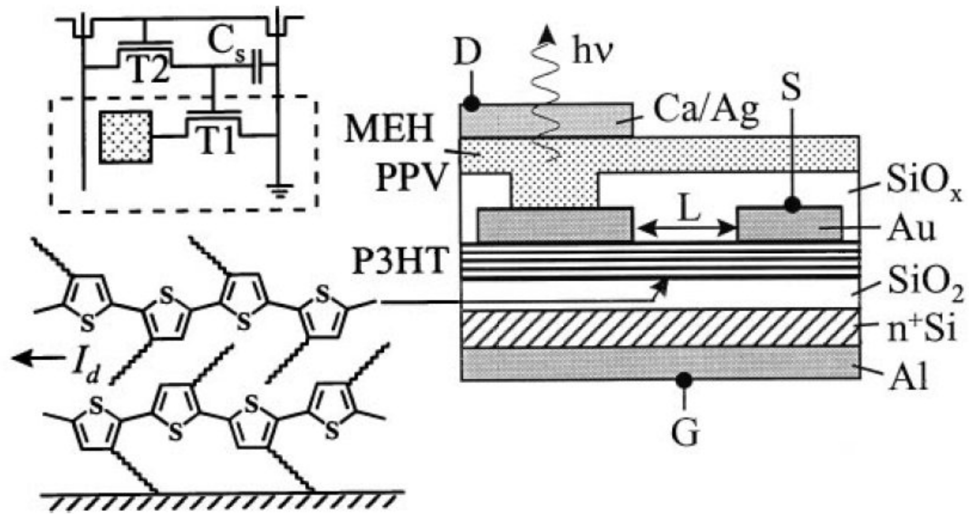


Figure 2-3 Cross section of the integrated $P_3HT$ FET and MEH-PPV LED. The device is a part (shown inside the dashed area in the top left corner) of a full active-matrix polymer LED pixel. The lamellar structure of the regioregular $P_3HT$ and its orientation relative to the $SiO_2$ substrate and the direction of the in-plane FET current *I*d is shown schematically.

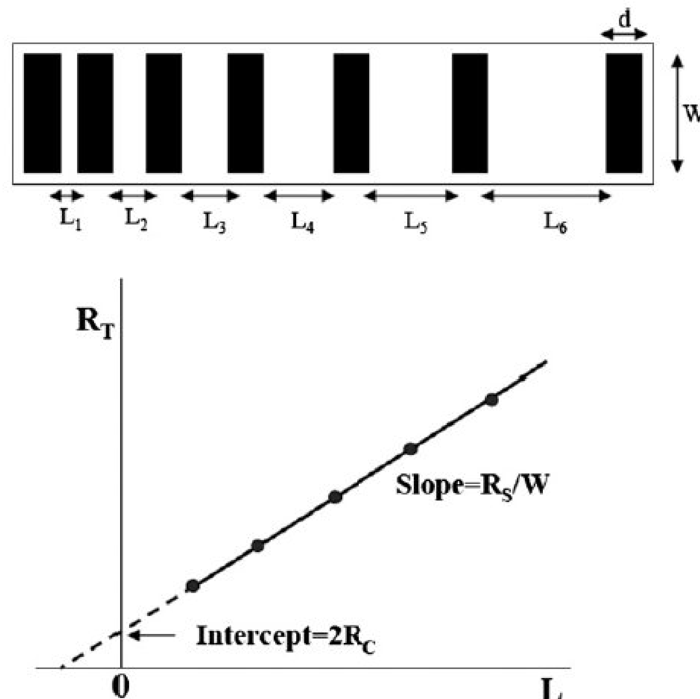


Figure 2-4 A transfer length method test structure and a plot of total resistance as a function of contact spacing, L.

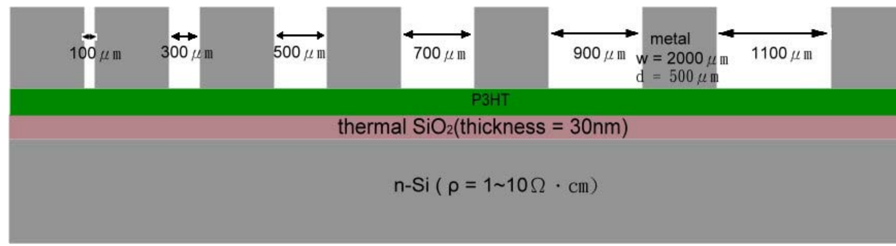


Figure 2-5 Cross-section of an actual test structure of contact resistance in this study.

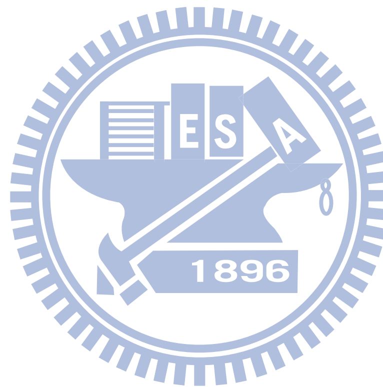

# Chapter 3 Results and discussion

## 3.1 The influence of leakage current on performance curve

Leakage current can have a significant impact on performance of OTFTs. In this section, we had adequately explained the origin of leakage current on OTFTs, and rigorously analyzed the distortion on performance curve. Additionally, methods of measurement, and the systematic comparison of the patterned active region and the lack one on leakage current had mentioned.

### 3.1.1 The adverse impact on output characteristics curve

Fig. 3-1(a) shows an output characteristics curve of our device which without patterning the active layer (W/L = 1600/200μm). It is observed that all the $I_D$ curves didn't approximate zero at $V_D$ = 0V. In this respect, we showed an expanded figure in Fig. 3-1(b) to obtain a clear observation. In ideal, if the $V_D$ = 0V, it should not be appeared current due to the lack of electric field between source/drain electrodes. However, we found that the $I_D$ curves increased toward the positive as the $|V_G|$ increased while $|V_D| \rightarrow 0$. The origin of $I_D$ offset was attributed to the electric field between drain electrode and gate electrode. When $V_D$ = 0V, drain electrode had been the highest potential in this system and then would induce a leakage current ($I_{D\ leakage}$) from drain electrode toward gate electrode, and caused a positive shift in $I_D$ curve. Because the $I_{D\ leakage}$ was following to the gate electrode, so we could use the $I_G$ to monitor the influence of $I_{D\ leakage}$ on output characteristics curve.

As can be seen in Fig. 3-1(c), $I_G$ (The negative quantity indicated that the current flowed toward the gate electrode) exhibited a dramatic increase while $V_D$ closed to 0V. In other words, the influence of gate current on output characteristics curve was more violent while $V_D$ closed to 0V. But on the other hand, the curve of $V_G$ = -20V indicated $I_G$ = -1E-8A at $V_D$ = -20V. It was attributed to the leakage current ($I_{S\ leakage}$) due to the electric field between source

electrode and gate electrode, and further, the possible relationship of current between source/drain electrodes and gate electrode could be given by

$$I_S = I_{Sleakage} + I_{DS} \quad (3\text{-}1)$$

$$I_D = -I_{DS} + I_{Dleakage} \quad (3\text{-}2)$$

$$I_G = -I_{Sleakage} + (-I_{Dleakage}) \quad (3\text{-}3)$$

where the minus means that the current flows into electrode.

In order to obtain clear observation in $I_{S\ leakage}$, we took the minus sign in $I_S$, and illustrated together with the $I_D$ in the Fig. 3-1(d). As the figure shows, $I_S$ did not approach $I_D$ in the entire curve. In ideal, the $I_S$ must be identical with $I_D$. This is because parts of current, which flowed from source electrode, flowed into the gate electrode.

Fig. 3-2(a) shows a transfer characteristics curve which measured as the same device in Fig. 3-1. In ideal, the channel should not accumulate charges at $V_G$ = 0V, but it is observed that the $I_D$ curves had a negative increment while $V_G$ approached 0V. The origin of negative shift in $I_D$ curve is attributed to the following reasons:

1. The leakage current ($I_{D\ leakage}$) due to the electric field between drain electrode and gate electrode.
2. The leakage current ($I_{DS\ leakage}$) due to the electric field between source electrode and drain electrode.

Comparing the $I_{D\ leakage}$ with $I_{D\ leakage}$ that mentioned in Fig. 3-1, the two leakages flow had opposite direction, and this direction of current flow, which flowing into drain electrode, led to a negative shift in $I_D$ curve. Secondly, the $I_{DS\ leakage}$ most likely correlated with the quality of organic active layer.

On the other hand, the shift of $I_D$ curve while $V_G$ approached 0V would attract adverse impact in device characteristics. In general, the $I_D$ numeral must be modulated with modulus, and illustrate transfer curve with logarithm scale while we characterizes the performance of a device. As can be seen in Fig. 3-2(b), if the $I_D$ curve had negative increase while $V_G$ approached 0V, the off state current ($I_D$ current when $V_G$ approached 0V) would increase.

If the off-state current had positive shift, on/off ratio would decreased.

Additionally, in contrast with output characteristics curve, we also illustrated the $I_G$ and $I_D + I_S$ curve in Fig. 3-2(c) / (d). As can be seen in Fig. 3-2(c), the $I_G$ decreased as the $|V_G|$ increased. In other words, the influence of $I_{D\ leakage}$ on transfer characteristics curve was more violent while $V_G$ closed to 0V. But on the other hand, we found that $I_G$ had a negative quantity while $|V_G|$ around surmounted 6V. This is attributed to the $I_{S\ leakage}$, which flowed into gate electrode, and the two opposite direction of current in gate electrode caused positive, negative numerals that varied according to $|V_G|$. In this respect, we had illustrated the current of source + drain electrodes in Fig. 3-2(d). The difference of each $I_D/I_S$ agreed with the existence of $I_{S\ leakage}$.

### 3.1.2 The methods of measurement

Whereas the influence of leakage current on performance curve, we suggested several methods to measure the leakage current as follows:

1. The measurement of $I_{DS\ leakage}$: As can be seen in Fig. 3-3, the gate electrode was floated and the drain electrode was applied sweeping voltage (0~-20V), and then we measured the $I_D$ as $I_{DS\ leakage}$.
2. The measurement of $I_{G\ leakage}$: As shown in Fig. 3-4, the source/drain electrodes was grounded and the gate electrode was applied sweeping voltage (0~-20V), and then we measured the $I_G$ as $I_{G\ leakage}$.
3. The measurement of $I_{D\ leakage}/I_{S\ leakage}$: As illustration in Fig. 3-5(a), the drain electrode was grounded and source electrode was floated, and after applying the sweeping voltage (0~-20V) at gate electrode, we measured the $I_D$ as $I_{D\ leakage}$. At the opposite steps of measurement, the $I_{S\ leakage}$ was measured and illustrated in Fig. 3-5(b). Although the $I_{S\ leakage}$ did not have direct impact on performance curve, it could be used to critically analyze the uniformity of one transistor on a die.

### 3.1.3 The examination of difference on leakage current between patterning active layer and without

As the origin of leakage current, which had mentioned in section 3.1.1, the device would compare with the device that had patterned active layer. Fig. 3-6(a) shows the output characteristics curve of a device which had the same W/L ratio as the device in Fig. 3-1, and the organic active layer had been patterned. Apparently, the phenomenon of distortion was reduced, and we could obtain a clear observation in the expand illustration in Fig. 3-6(b). In regard to the reduction of distorted phenomenon on curve, it was attributed to the reduction of disordered leakage path after patterning the organic active layer, and it was confirmed in Fig. 3-6(d), which we used the third method of measurement in section 3.1.2. Additionally, for comparison with Fig. 3-1(a) in Fig. 3-6(c), it is observed that the on-current of the patterned device was less than the without patterning one. The gate electrode of device was not patterned, so the active layer would be induced charges everywhere, and the on-current would reduced as the area of organic active layer decreased.

In contrast to Fig. 3-1(c), the $I_G$-$V_D$ curve was shown in Fig. 3-7(a). As the illustration, $I_G$ had been compressed with patterning the active layer. Furthermore, we compared the gate current with Fig. 3-1(c), and illustrated in Fig. 3-7(b). It is clearly observed that $I_G$ was dramatically reduced wherever $V_G$ = 0V or -20V, and finally it was confirmed in Fig. 3-7(c), which we used the second method of measurement in section 3.1.2.

In contrast to Fig. 3-1(d), the $I_D + I_S$-$V_D$ curve was shown in Fig. 3-8(a). As the illustration, the difference between $I_D$ and $I_S$ was decreased. It is attributed to the reduction of $I_{D\ leakage}$ and $I_{S\ leakage}$. As mention in Eq. (3-1) and Eq. (3-2), the difference of $I_D$ and $I_S$ were reduced as the $I_{D\ leakage}$ and $I_{S\ leakage}$ decreased. Furthermore, we compared the source current with Fig. 3-1(d), and illustrated in Fig. 3-8(b). It is clearly observed that $I_S$ was dramatically reduced wherever $V_G$ = 0V or -20V, and finally it was confirmed in Fig. 3-8(c), which we used the third method of measurement in section 3.1.2.

As shown in Fig. 3-9(a), a transfer characteristics curve with the same device as in Fig. 3-6 was observed that the negative increment while $V_G$ approached 0V was reduced. That is

to say that on/off ratio would be increased due to the reduction of off-current. As can be seen in Fig. 3-9(c), it is clearly observed, the on/off ratio had been conspicuously increased due to the reduction of disordered path of leakage. In contrast to Fig. 3-2(c), the $I_G$-$V_G$ curve was shown in Fig. 3-9(d), Fig. 3-9(e). As the illustration, the $I_G$ had been considerably decreased in comparison to without pattern. Finally we used the first method of measurement, which had been mentioned in section 3.1.2, to confirm it in Fig. 3-9(f).

## 3.2 The influence of surface treatment on leakage current

Fig. 3-10(a) and Fig. 3-10(b) show the output characteristics curve of OTFTs which consisted of treatment and without on the surface of gate insulator. For a comparison in Fig. 3-10(c), it is clearly observed, after treatment on surface of gate insulator, the on-current ($I_D$) was gradually increased by the more ordered organic active layer, yet the distortion of curves were also increased while $V_D$ approached 0V. As mentioned above, the origin of distortion on output characteristics curves were gate leakage current, so we showed the analysis of $I_G$ in Fig. 3-10(d). And it is confirmed that after treatment on surface of gate insulator, $I_G$ was increased.

Fig. 3-11(a) shows the transfer characteristics curve with the same device as in Fig. 3-10. Apparently, the off-state current, which $V_G$ approached 0V, was increased in comparison to the device without surface treatment.

Many researches indicate that the ordering of organic semiconductor material would be improved after a hydrophobic treatment on the surface of gate insulator [27-29]. But after we characterized the parameters in Fig. 3-11(b), we considered that the good ordering of organic material have higher mobility (The mobility of OTFTs with and without surface treatment are 0.004 ($cm^2V^{-1}s^{-1}$) and 0.0023 ($cm^2V^{-1}s^{-1}$) respectively.), whereas it would decrease the resistance between drain and gate insulator. Consequently, it would increase the gate leakage current.

On the other hand, as mentioned above, the second origin of leakage current had been directly compared with the device without treatment in Fig. 3-11(c). It is observed, $I_{DS\ leakage}$ was also increased obviously after surface treatment. In regard to the decrease of resistance

between drain and gate insulator, we had confirmed it in Fig. 3-11(d) by used the transfer length method. As the illustration, the slop of linear fit line had considerably decreased in comparison to the device without surface treatment. In other words, the decrease of sheet resistance (6.36 → 0.493 GΩ/square) between each electrode, which mentioned in Fig. 2-5, could clarify the increase of $I_{G\ leakage}$ and $I_{DS\ leakage}$. Furthermore, although the contact resistance was also decreased (176 → 42.7 MΩ) by surface treatment, we considered that the sheet resistance dominated the performance of our device because the distinct difference in resistance.

## 3.3 The influence of electrode metals on leakage current

Fig. 3-12(a) and Fig. 3-12(b) show the output characteristics curves of the OTFTs that the source/drain electrode consisted of Ti and Cr. Comparing with Ni in Fig. 3-12(c), it is clearly observed that the higher work function (Ti = 4.33, Cr=4.5, Ni=5.15eV) of metal had the higher on-current ($I_D$). However, as the illustration in Fig. 3-12(d), the current (leakage) of static state ($V_G$ = 0V) were also had positive relation with work function. As mentioned above, the origin of distortion on output characteristics curves had measured in Fig. 3-12(e). As the illustration, the higher $I_{D\ leakage}$ corresponded to the more distorted curve at static state in Fig. 3-12(c) (while $V_D$ approached 0V) and Fig. 3-12(d).

Fig. 3-13(a) and Fig. 3-13(c) show the transfer characteristics curves of the same device in Fig. 3-12(a) and Fig. 3-12(b). As the illustration, the distortion phenomenon of Cr electrode was more serious than Ti electrode. The excessive shift would cause the off-current increase, and consequently the on/off ratio would be decreased. Therefore after we characterized the curves in Fig. 3-13(b) and Fig. 3-13(d) and then compared with Ni in Fig. 3-13(e). Contrary to the expectation, the on/off ratio of Cr electrode was greater than Ni electrode (Ni = 125, Cr = 200), yet the Ti electrode had the smallest on/off ratio (Ti = 50) due to the excessively slight on-current (for μ: Ni = 0.00134, Cr = 0.001, and Ti = 0.00023 $cm^2V^{-1}s^{-1}$).

As mentioned above, the second origin (leakage current), which caused the distortion of

transfer characteristics curve, had been compared with the Ni electrode in Fig. 3-13(f). As the illustration, the magnitude of $I_{DS\ leakage}$ exactly confirmed the magnitude of off-current in Fig. 3-13(e).

Additionally, the different metals of electrode also had the impact on threshold voltage. After characterized the curves in Fig. 3-13(e), we obtained the $V_{th}$ of devices with variety of electrode metals as Ni = 3.63V, Cr = -7.51V, and Ti = -10.78V. In regard to the shift of $V_{th}$, we had measured the contact resistance to clarify the reason. As illustration in Fig. 3-13(g), the three contact resistances was extracted as Ni = 18MΩ, Cr = 730MΩ, and Ti = 2.7GΩ at quite approximate slop of linear fit line (for $R_s$: Ni=0.636, Cr=0.728, and Ti = 0.694 ×1E10Ω/□). In other words, the channel of device, which had the higher contact resistance between electrode/semiconductor, would be distributed the lower voltage at the same potential between source and drain electrodes ($V_{DS}$). Consequently, the higher contact resistance device needed the higher voltage to "turn on" the channel.

Many researches indicate that choosing a material that has high work function close to the highest occupied molecular orbital (HOMO) level of a p-type semiconductor could reduce the hole-injection barrier [30-32]. But after we characterized the variety of metals in Fig. 3-14(a) and arranged data in table 3-1, we considered that the interface properties could not be predict solely on work function of metals and the ionization potential (IP) of organic semiconductors, whereas the contact resistance could be used to monitor the interface properties, and it had the inverse proportion to leakage current as shown in Fig. 3-14(b).

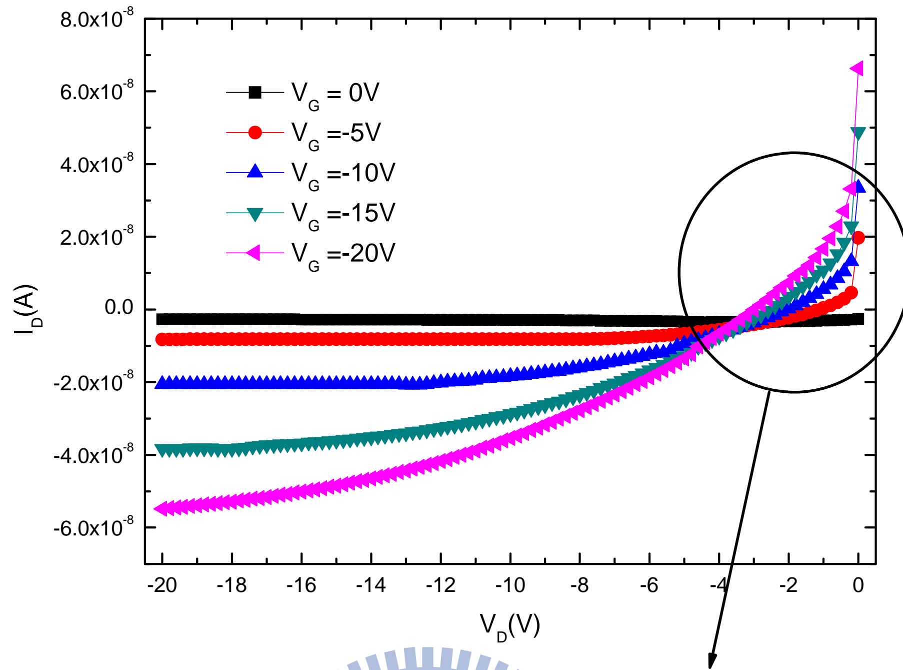


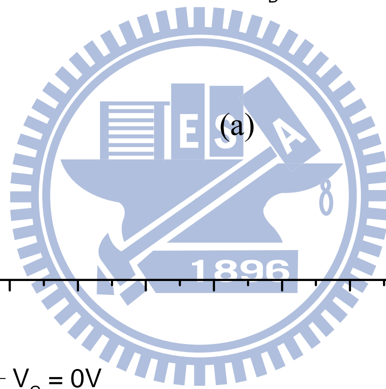

(a)

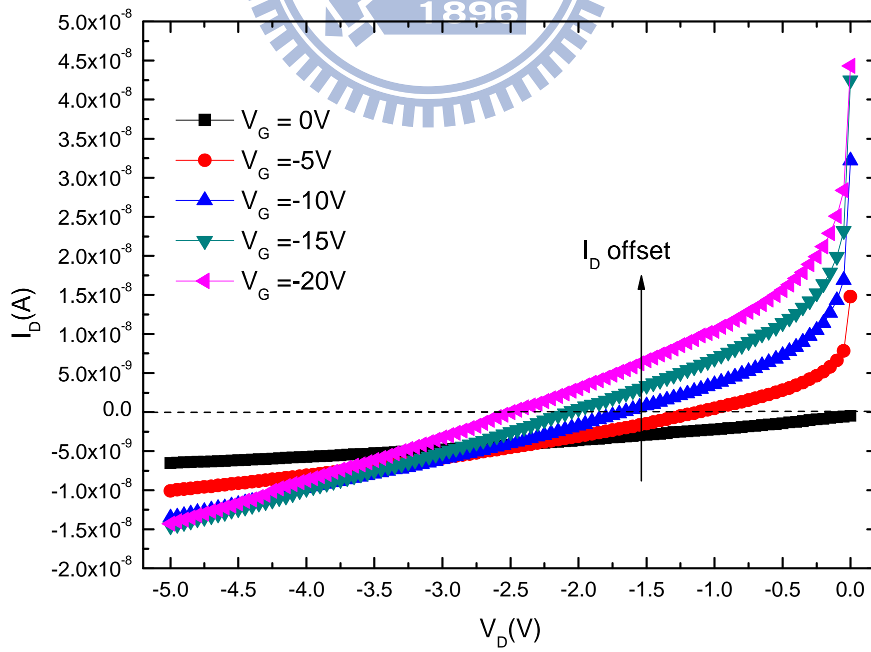


(b)

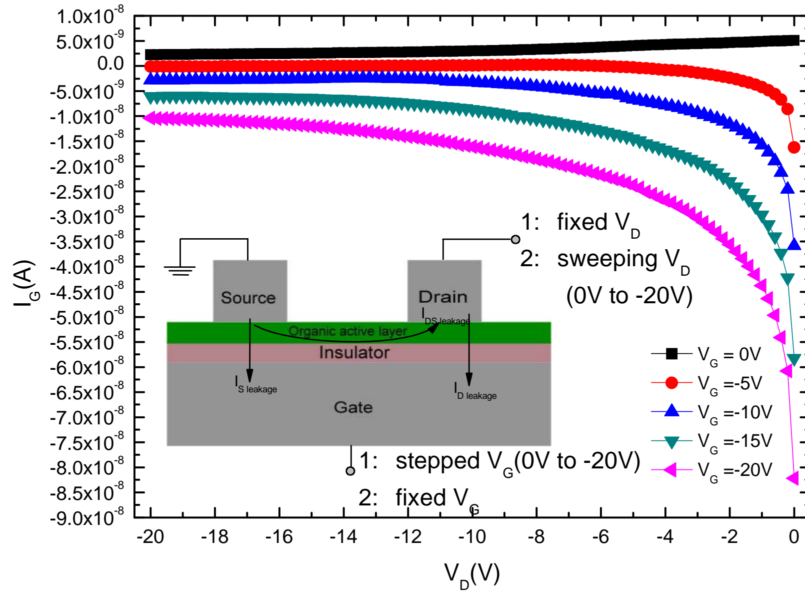


(c)

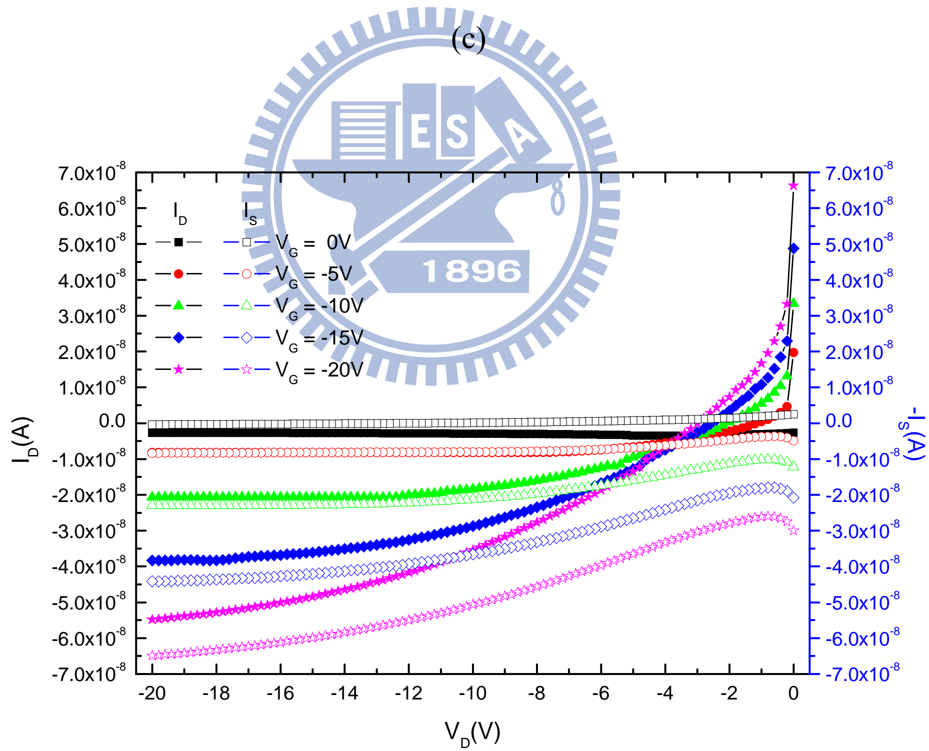


(d)

Figure 3-1 The performance curves of OTFTs (W/L = 1600/200 μm, w/o pattern) as: (a) output characteristic curves, (b) expanded $I_D$-$V_D$ curves, (c) $I_G$-$V_D$ curves, (d) $I_S$ & $I_D$-$V_D$ curves.

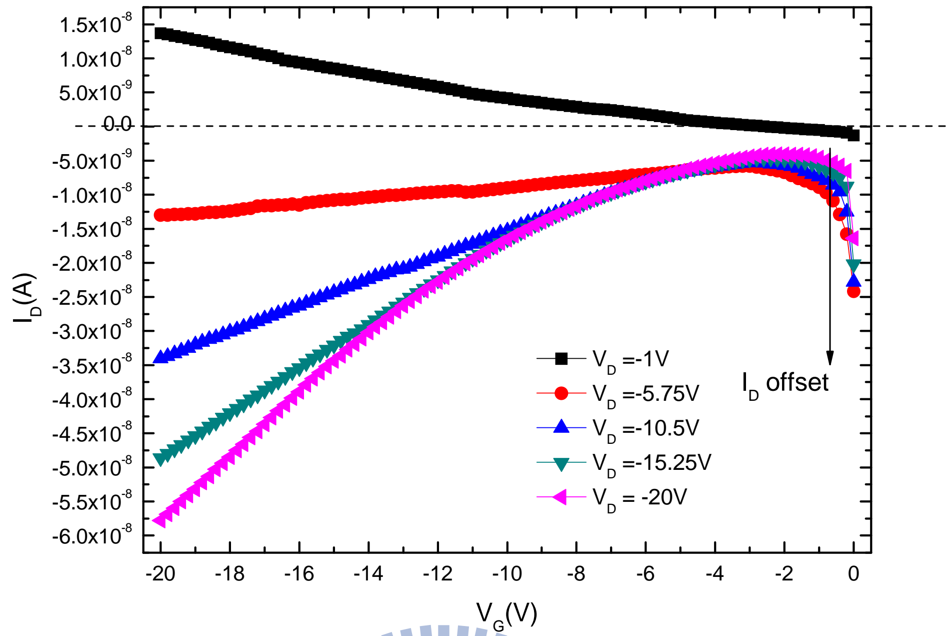


(a)

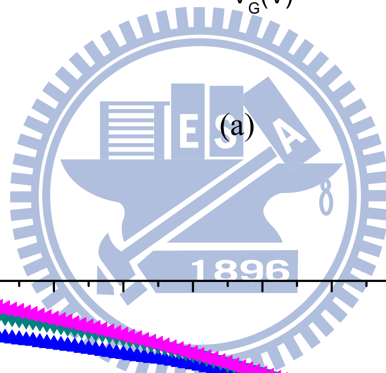


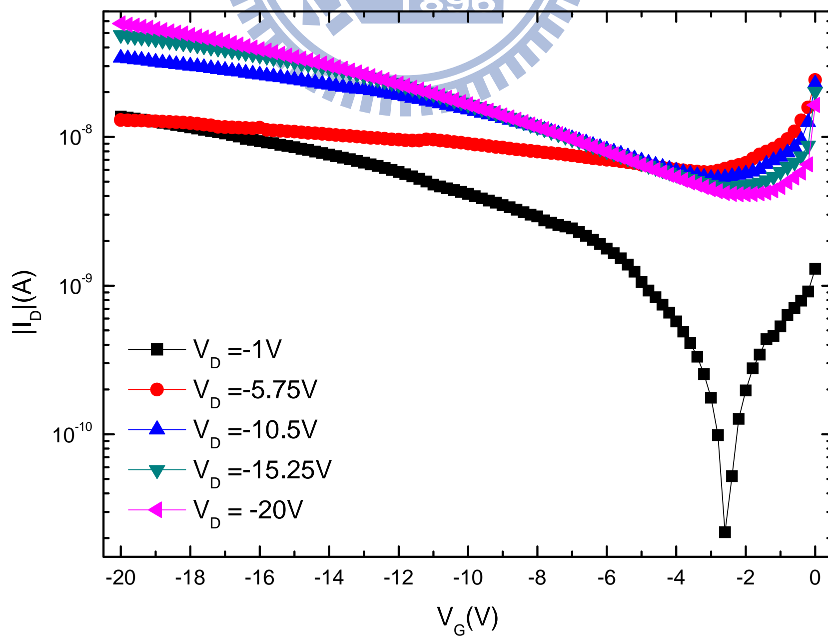


(b)

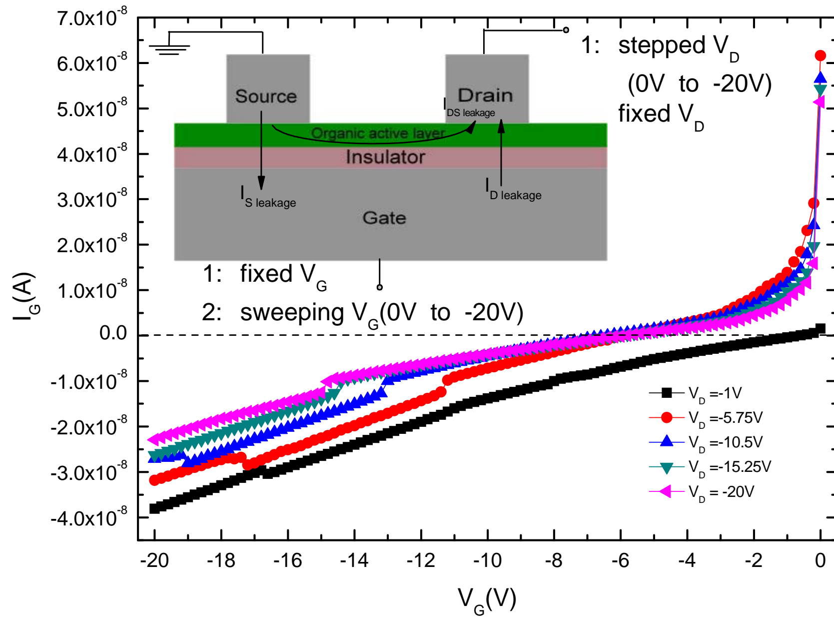


(c)

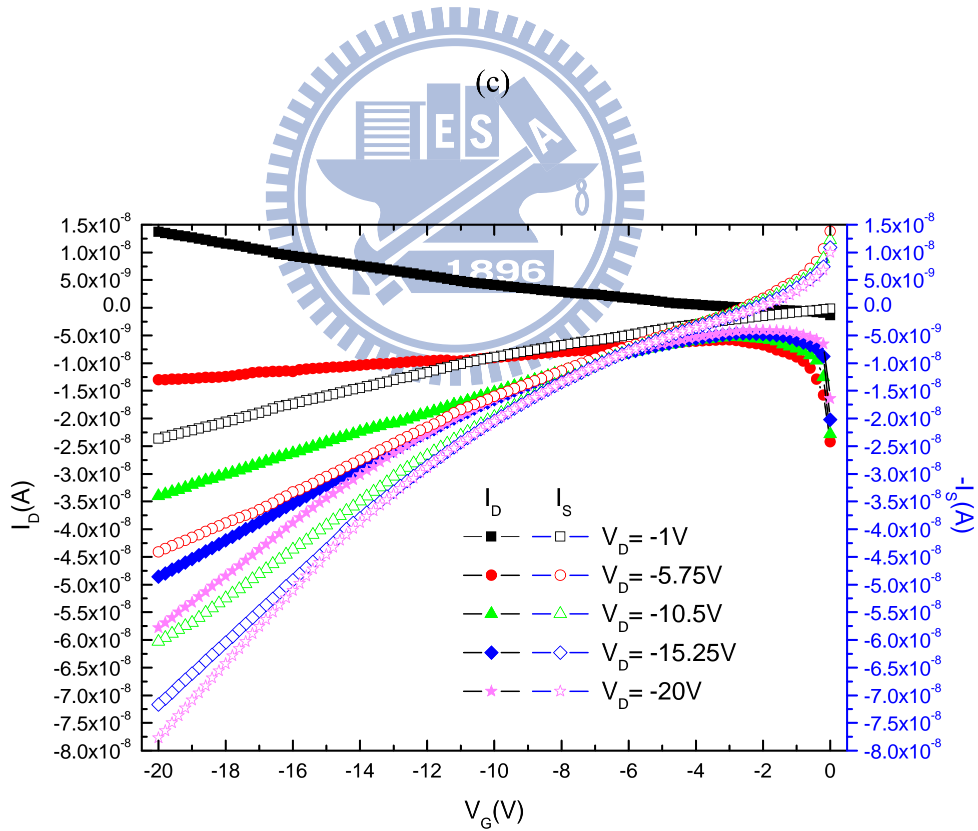


(d)

Figure 3-2 The performance curves of OTFTs with the same device as in Fig. 3-1： (a) transfer characteristic curves, (b) $|I_D|$-$V_G$ curves, (c) $I_G$-$V_G$ curves, (d) $I_D$ & $I_S$-$V_G$ curves.

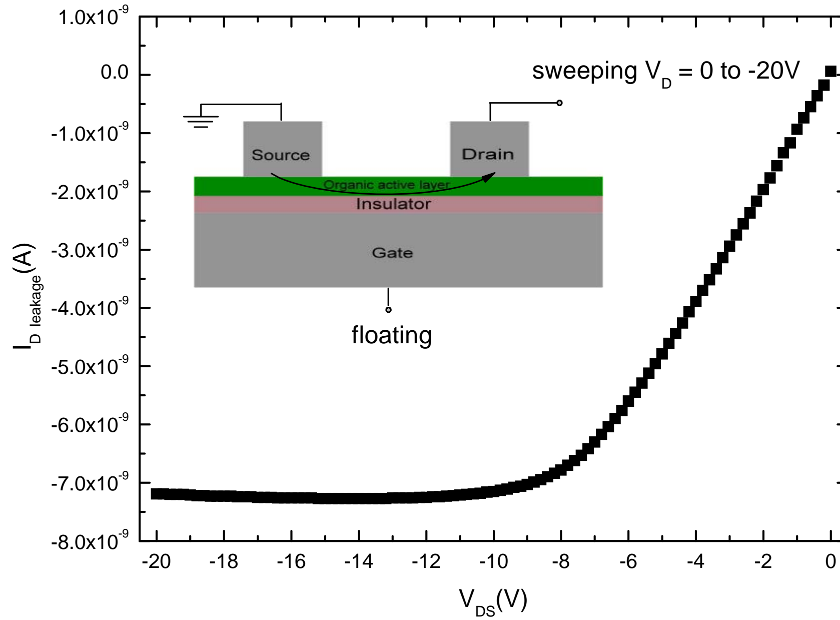


Figure 3-3 The curve of $I_{DS\ leakage}$ while gate electrode is floated, and the embedded diagram is leakage current schema.

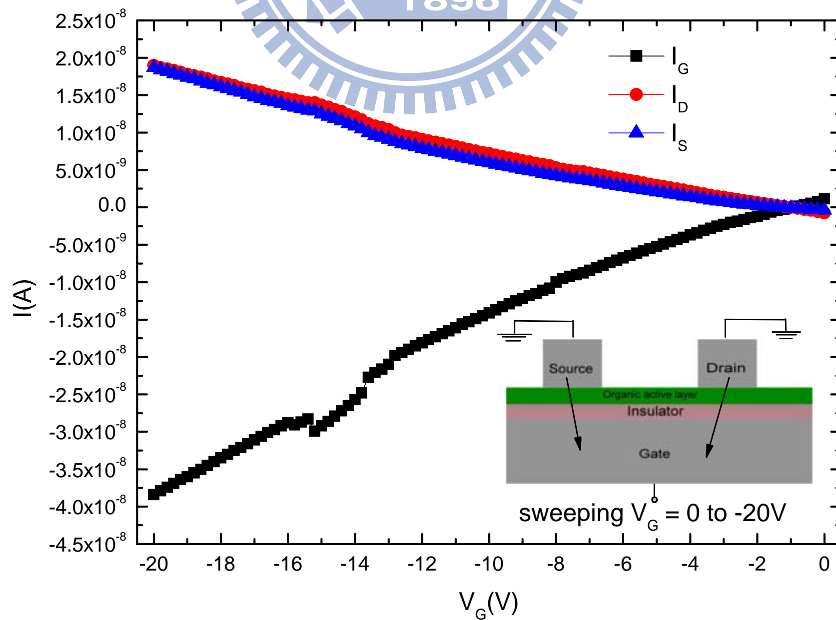


Figure 3-4 The curves of $I_{G\ leakage}$, and the embedded diagram is gate leakage current schema. As the illustration, due to the uniformity of a transistor on a die, $I_G \fallingdotseq 2I_D$ ($I_D \fallingdotseq I_S$).

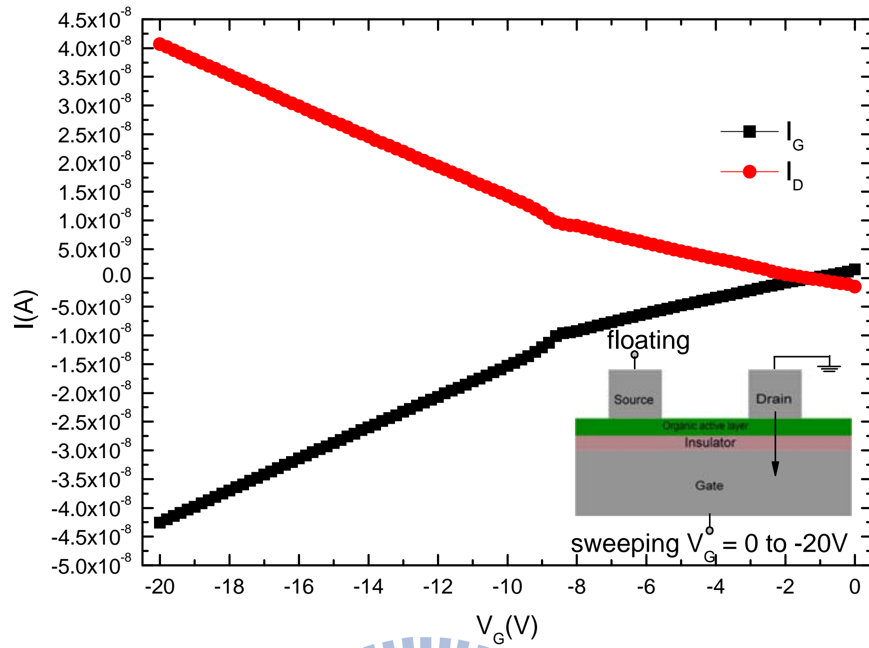


(a)

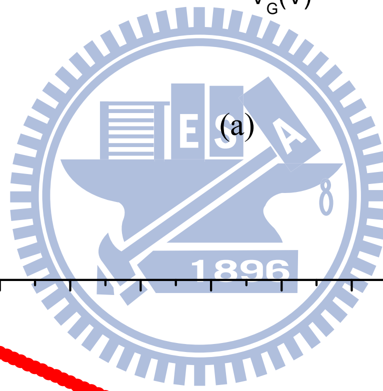


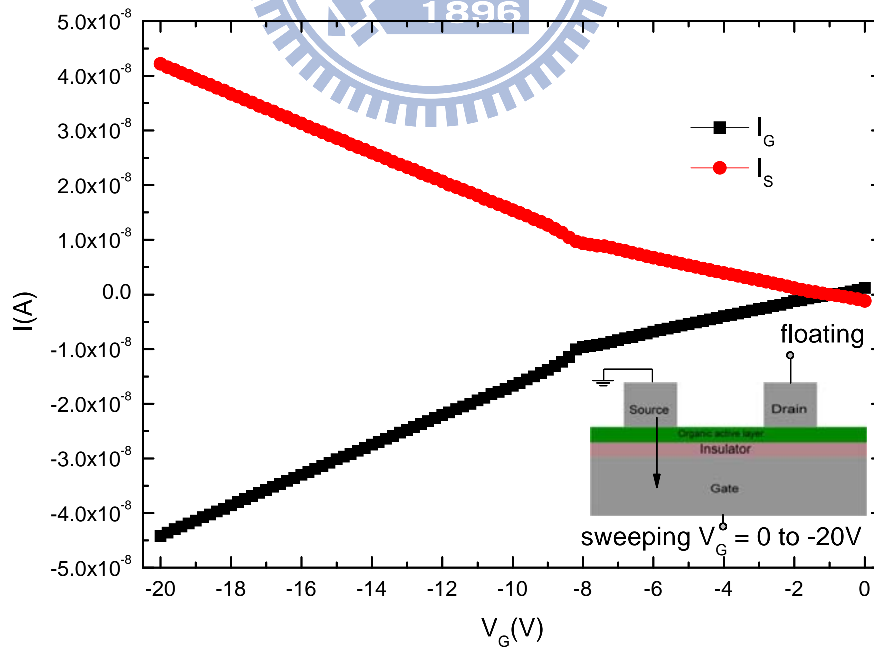


(b)

Figure 3-5 The curves of (a) $I_{D\ leakage}$ and (b) $I_{S\ leakage}$.

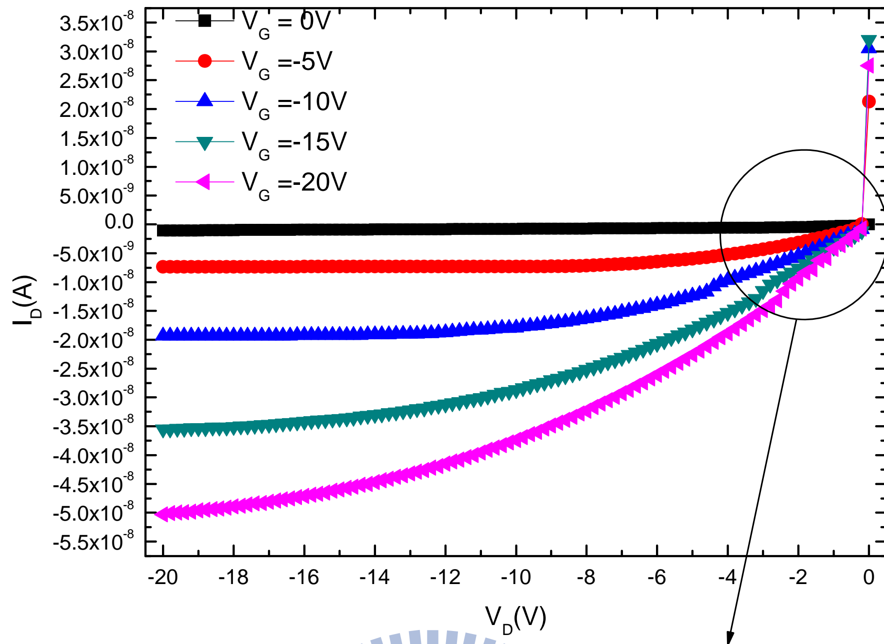


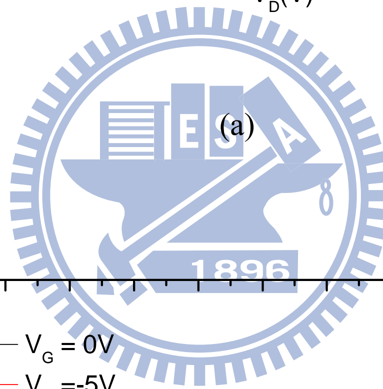

(a)

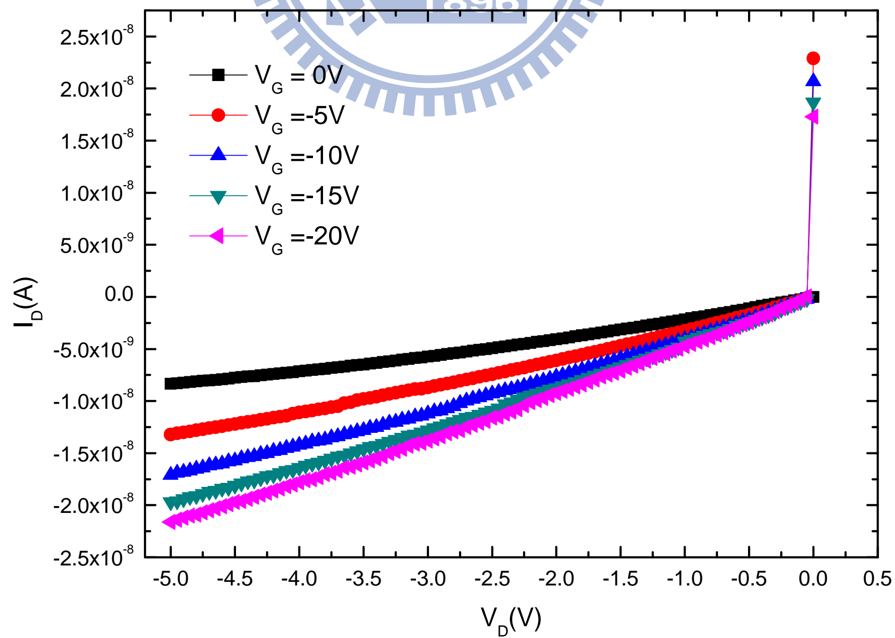


(b)

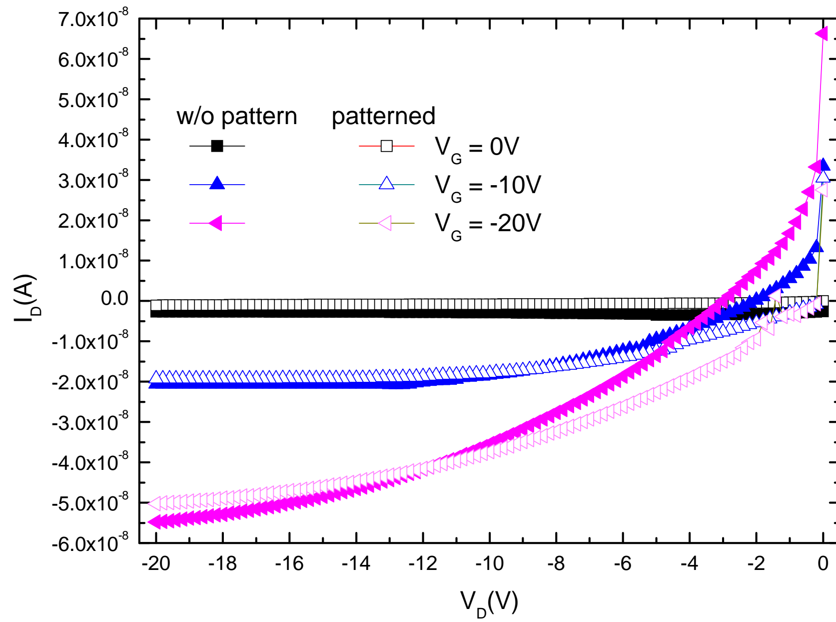


(c)

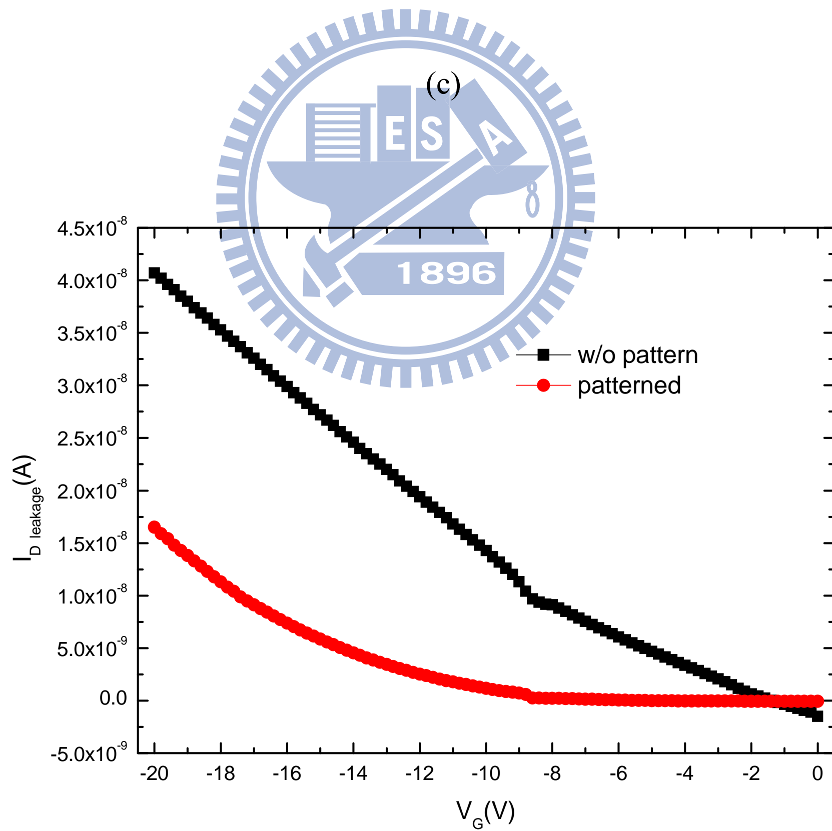


(d)

Figure 3-6 The performance curves of OTFTs (with pattern) with the same W/L ratio as in Fig. 3-1 as: (a) output characteristic curves, (b) expanded $I_D$-$V_D$ curves, (c) comparing with Fig. 3-1(a), (d) comparison of $I_{D\ leakage}$.

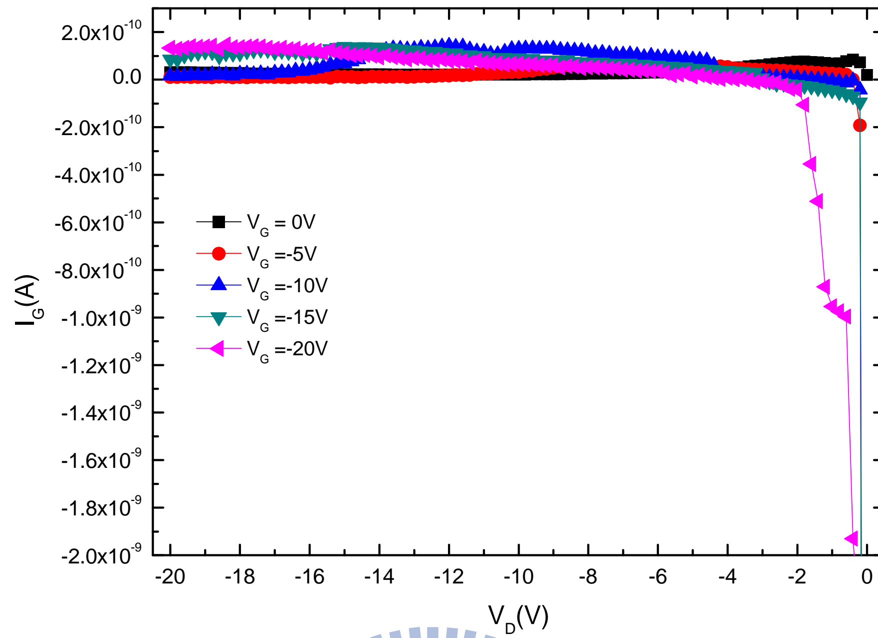


(a)

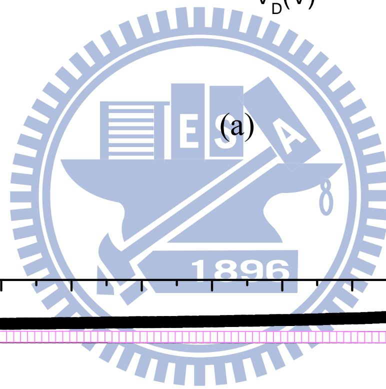
1896

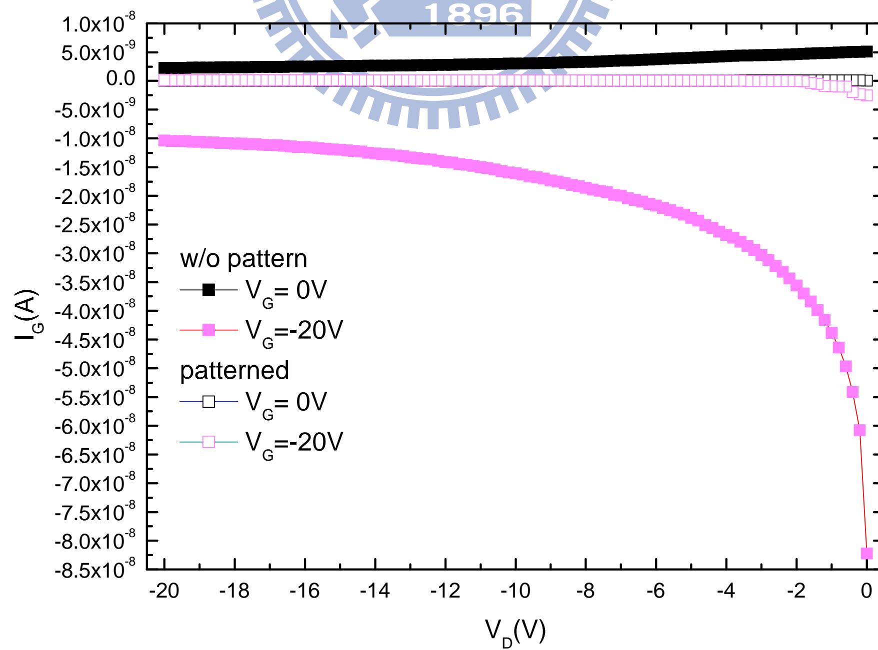


(b)

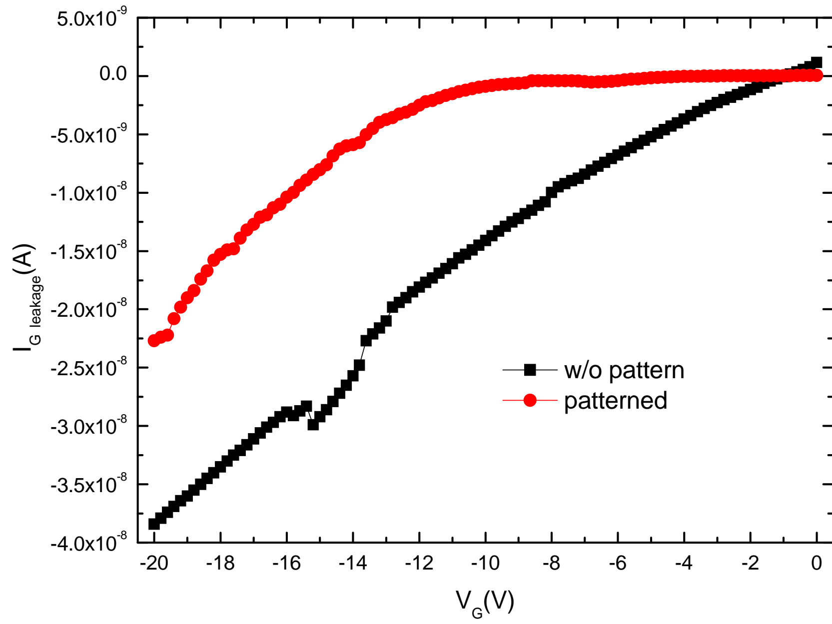


(c)

Figure 3-7 The curves of (a) $I_G$-$V_D$ (with pattern), (b) comparison of $I_G$-$V_D$, (c) comparison of $I_{G\ leakage}$.

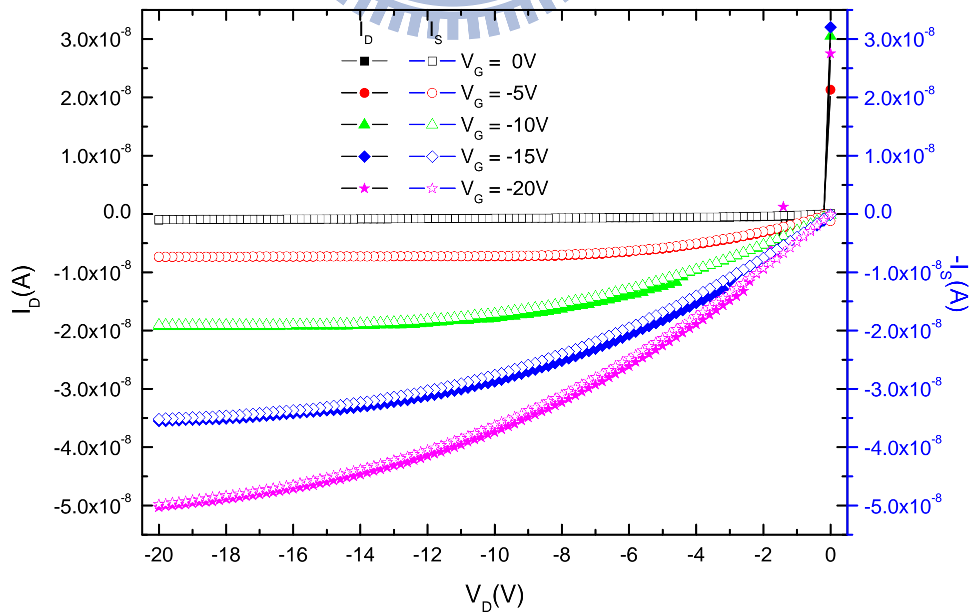


(a)

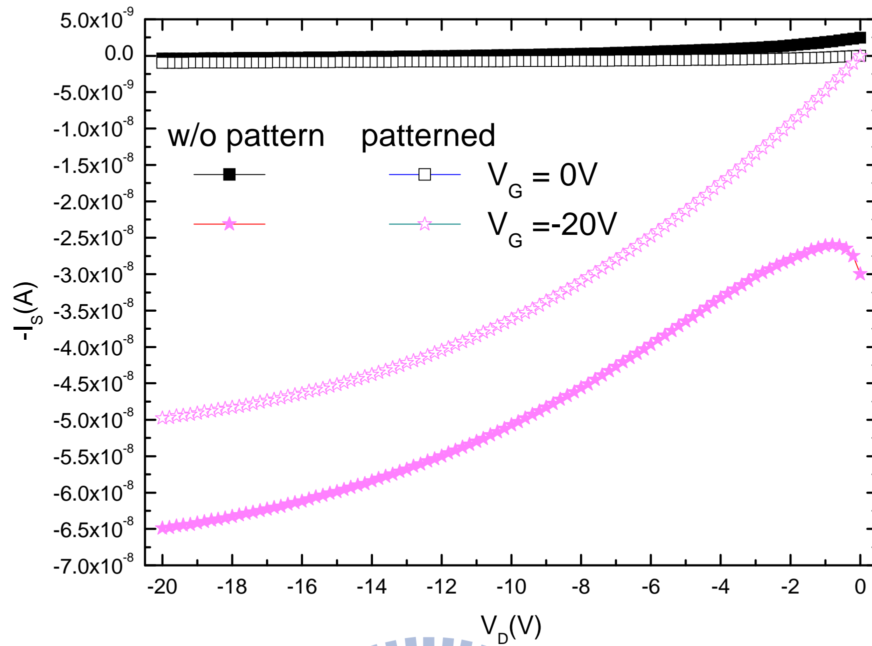


(b)

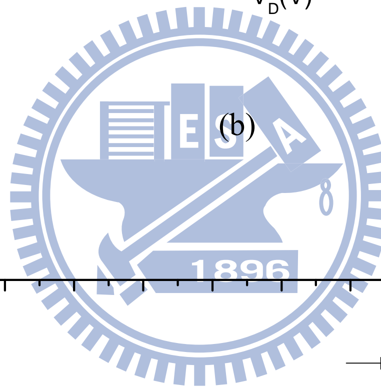

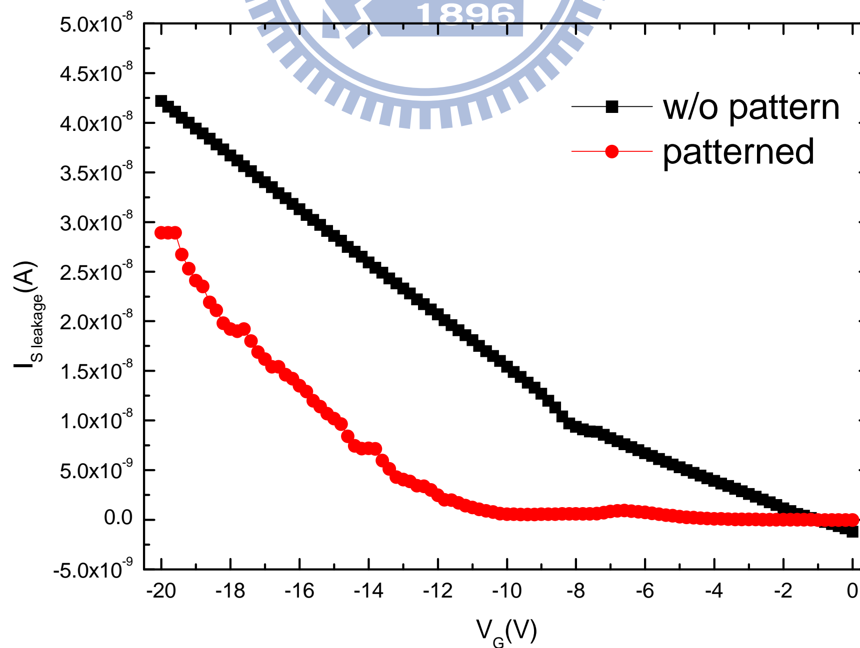


(c)

Figure 3-8 The curves of (a) $I_D$ & $I_S$-$V_D$, (b) comparison of $I_S$, (c) comparison of $I_{S\ leakage}$.

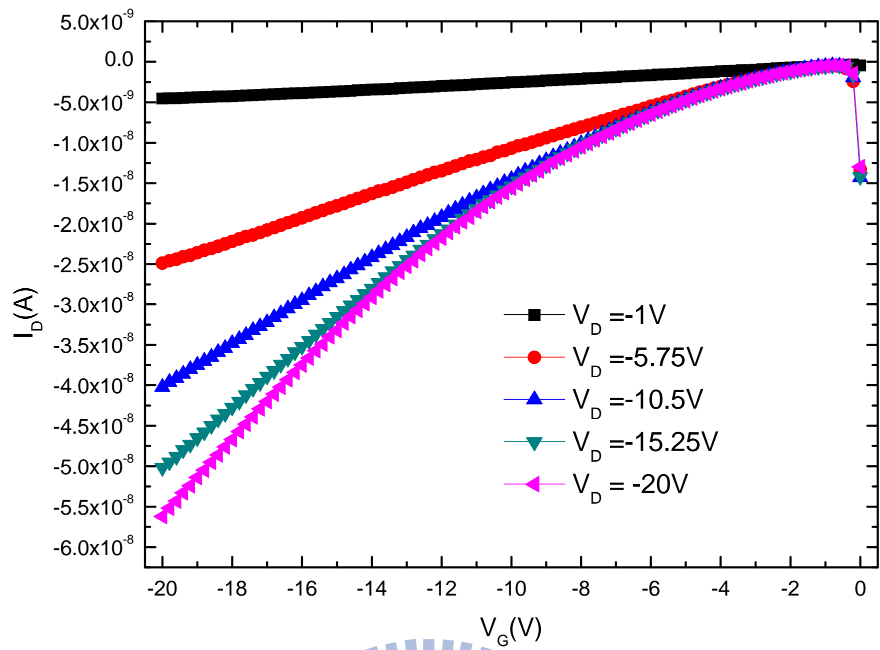


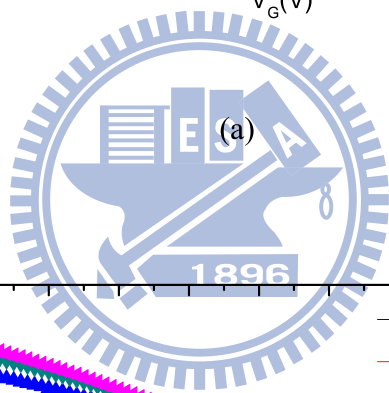


(a)

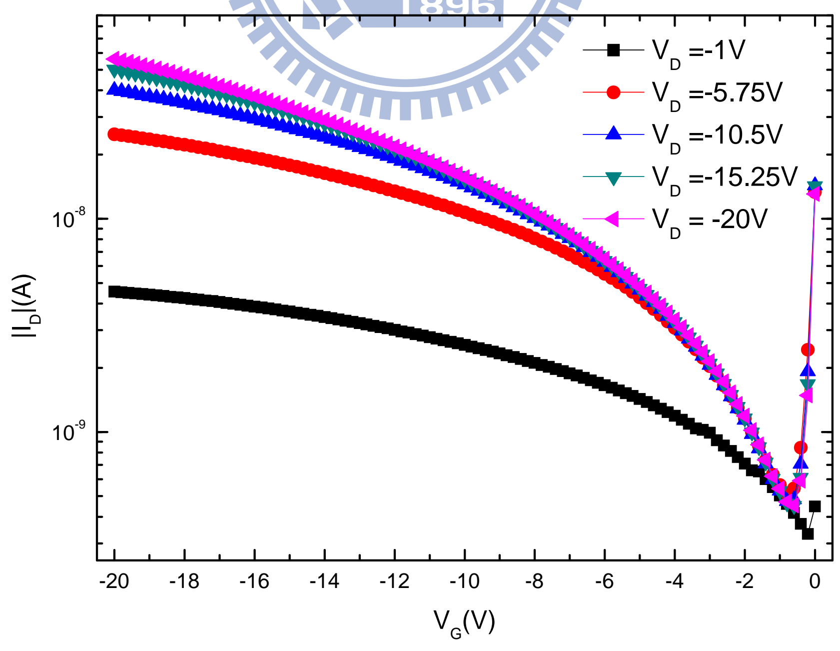


(b)

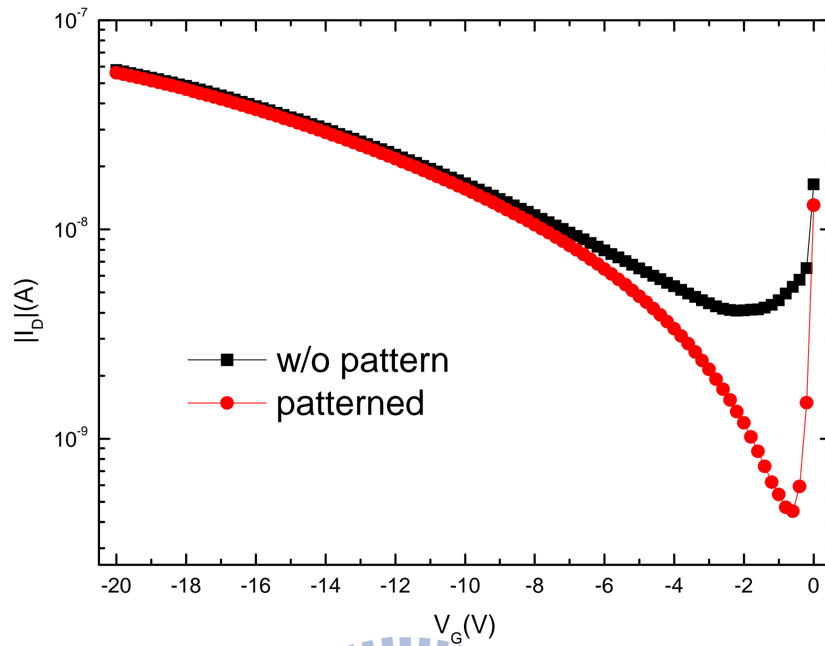


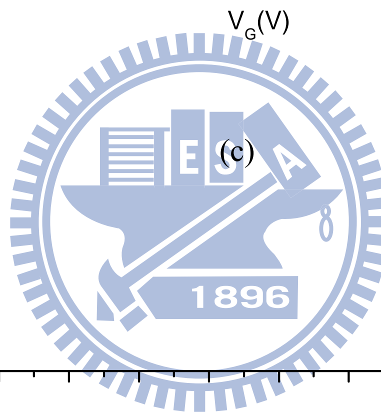

(c)

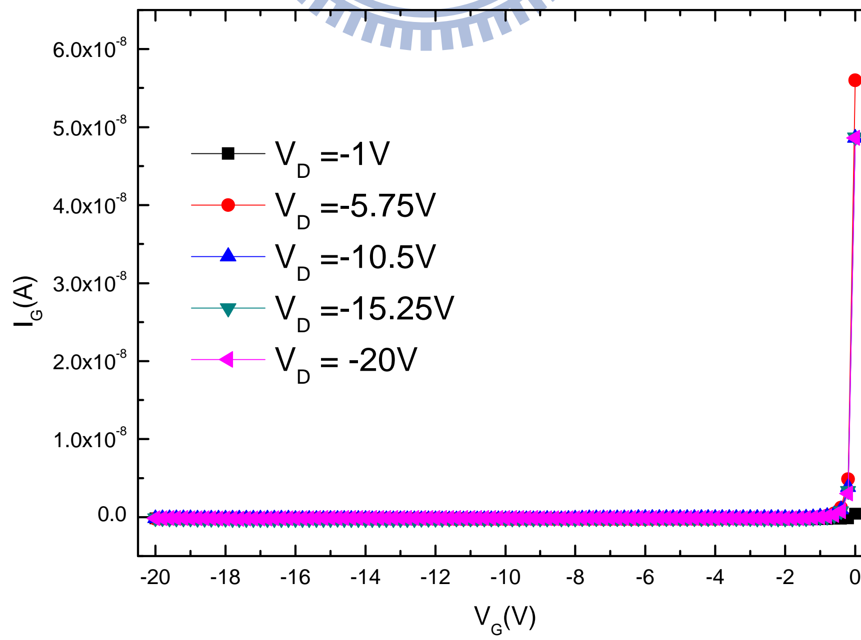


(d)

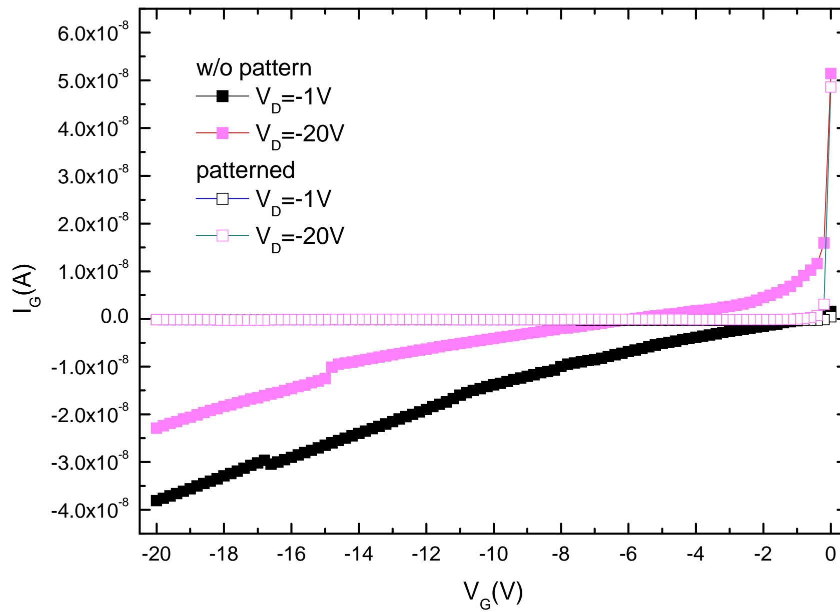


(e)

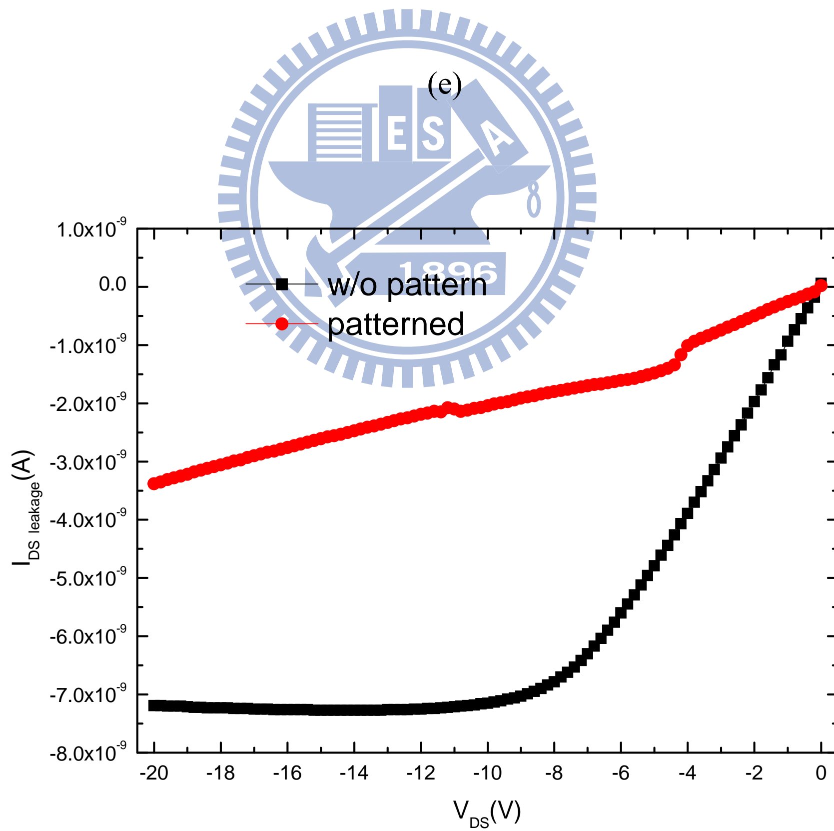


(f)

Figure 3-9 The performance curves with the same device as in W/L ratio as in Fig. 3-6 as: (a) transfer characteristic curves, (b) $|I_D|$-$V_G$ curves, (c) comparison of $|I_D|$-$V_G$ curves, (d) $I_G$-$V_G$ curves, (e) comparison of $I_G$-$V_G$ curves, (f) comparison of $I_{DS\ leakage}$.

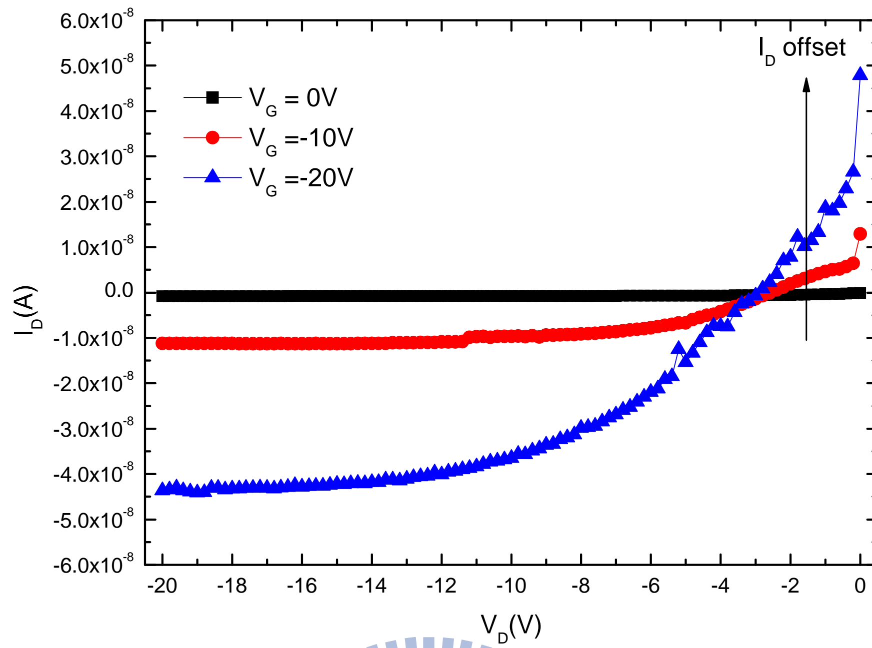


(a)

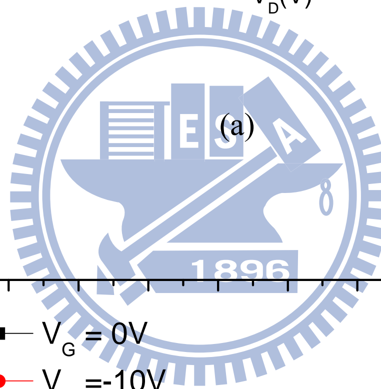

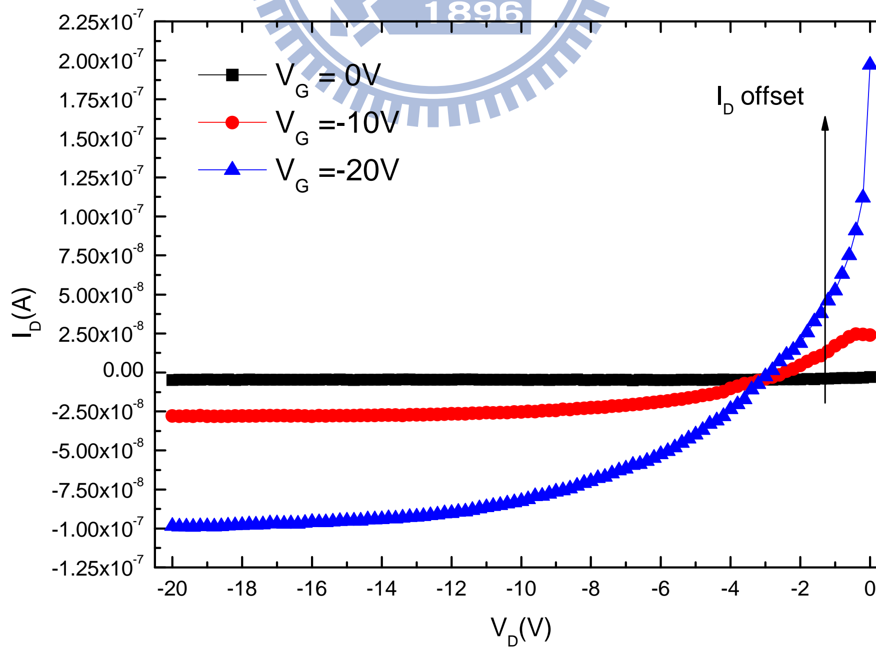


(b)

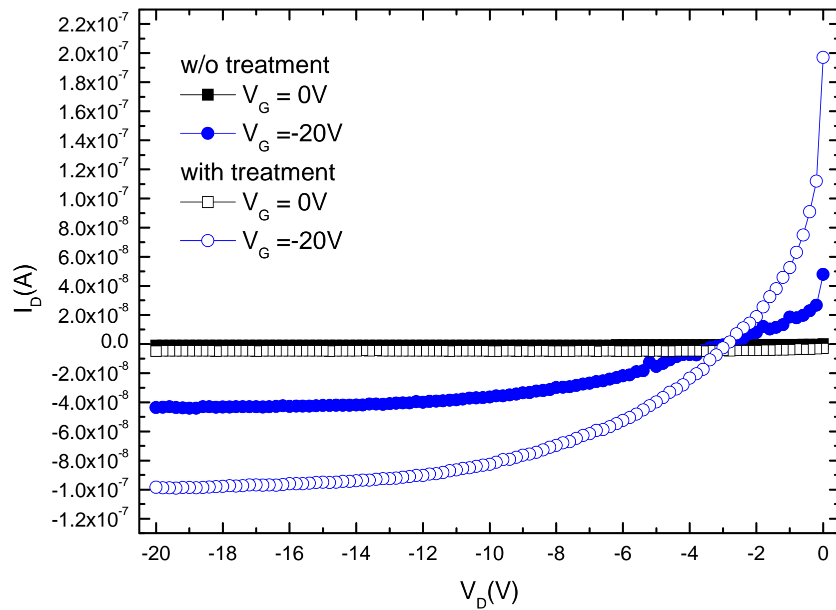


(c)

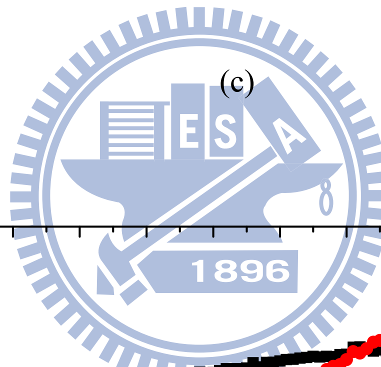
1896

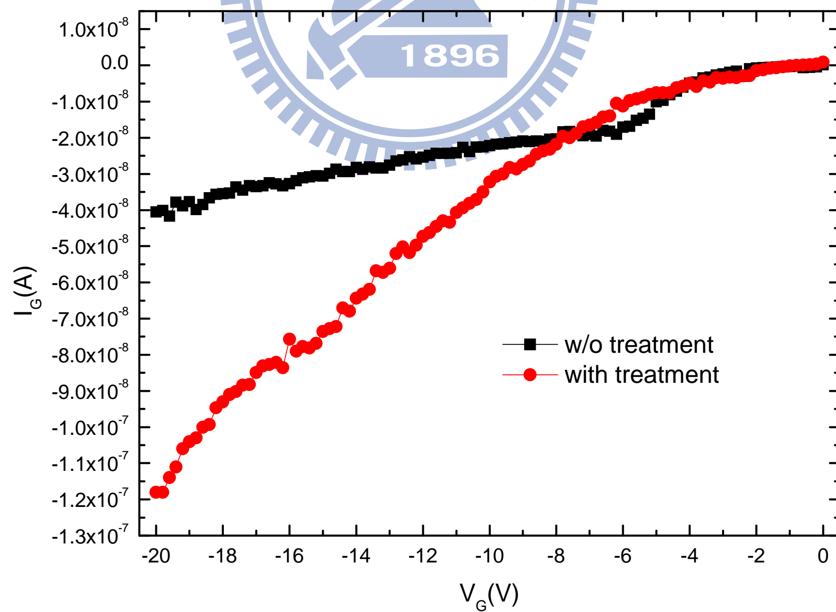


(d)

Figure 3-10 The output characteristic curves of OTFTs which consist of (a) lack of surface treatment, (b) with surface treatment, (c) comparison of (a) and (b), and (d) comparison of $I_{G\ leakage}$.

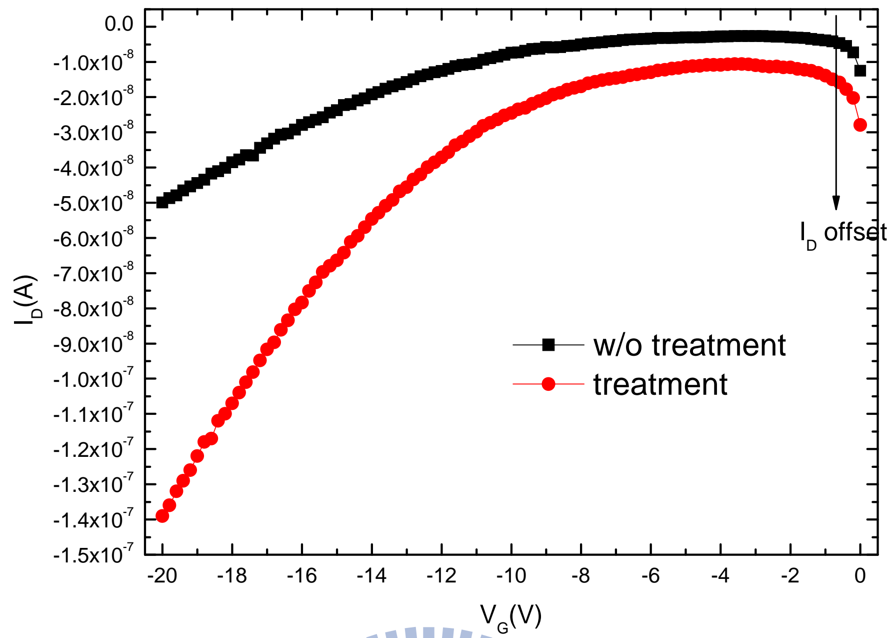


(a)

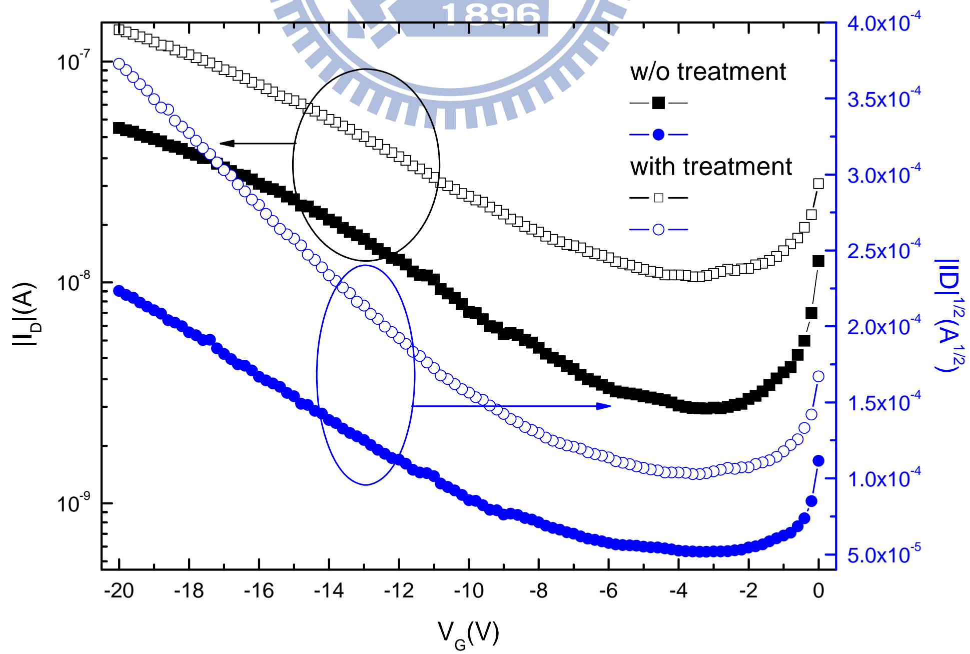


(b)

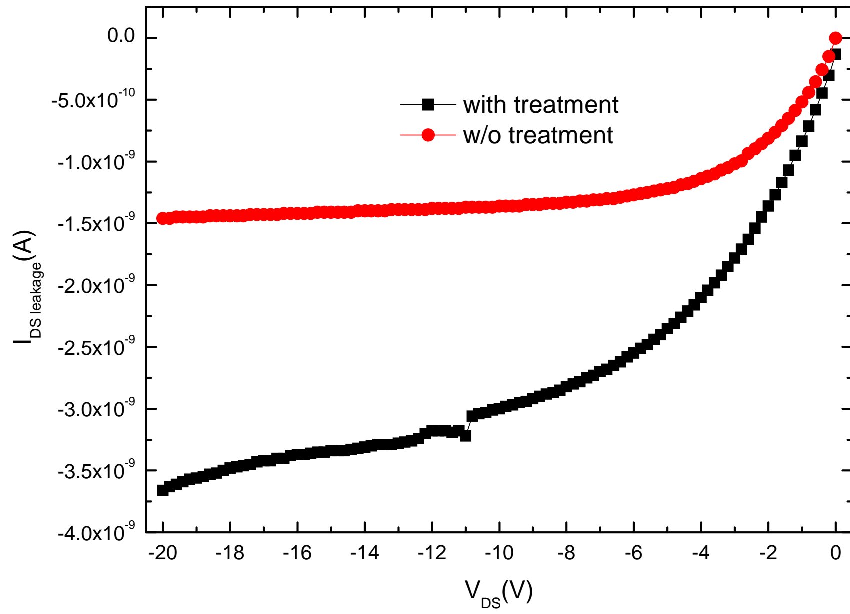


(c)

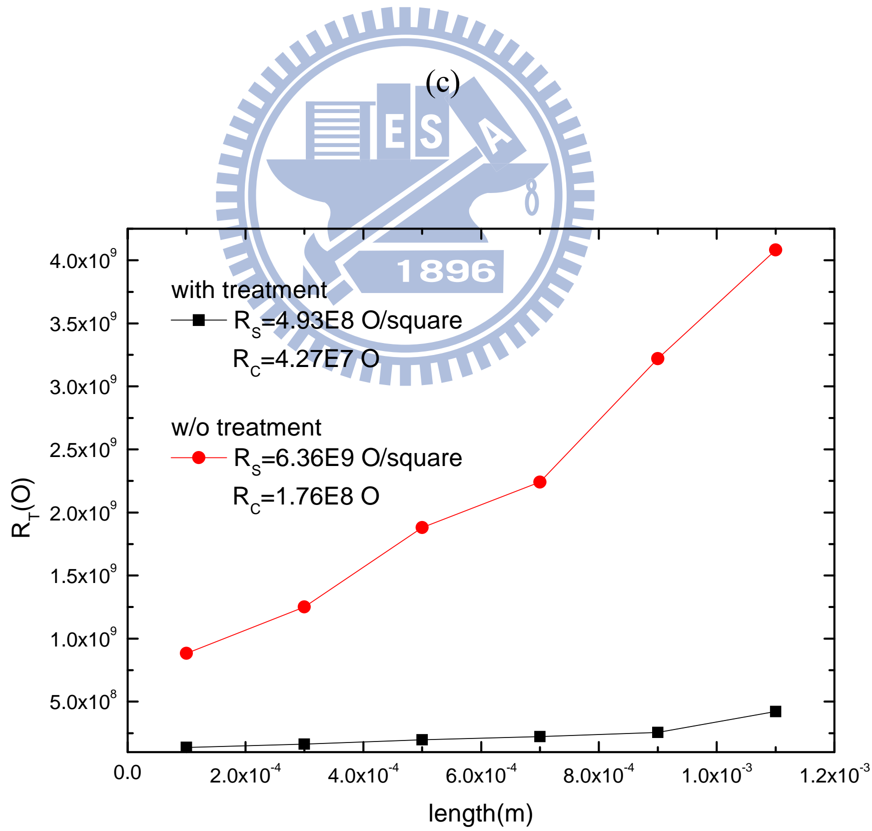


(d)

Figure 3-11 The transfer characteristic curves of OTFTs which consist of (a) comparison of ID-VG curves, (b) comparison of |ID|-VG curves, (c) comparison of IDS leakage, (d) comparison of total resistance ($R_T$) versus the length.

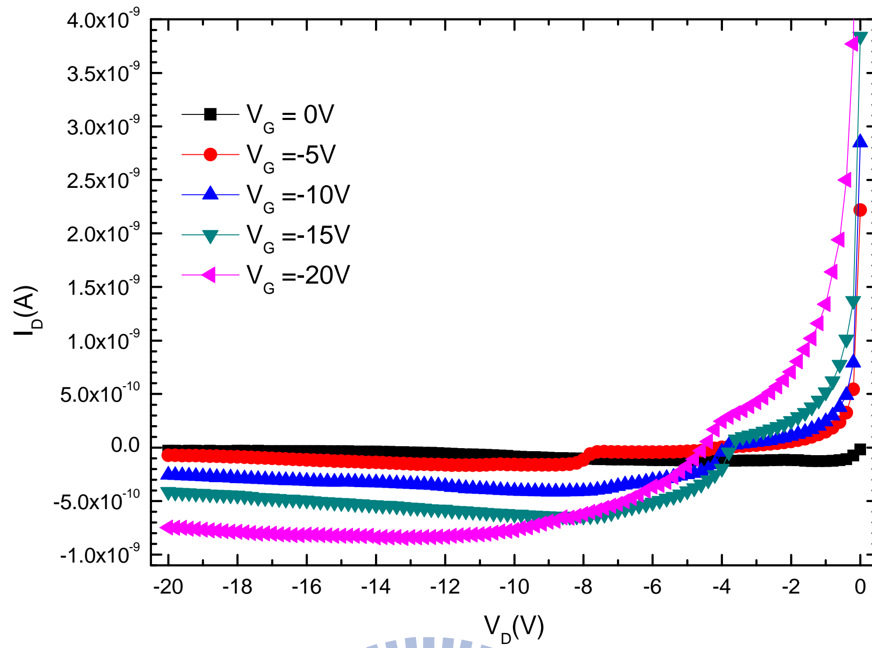


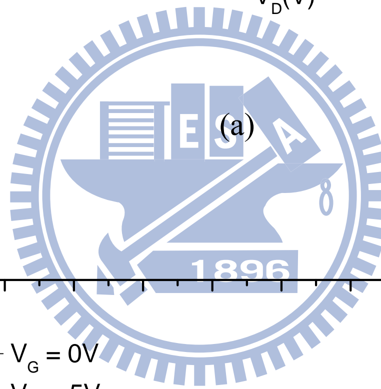

(a)

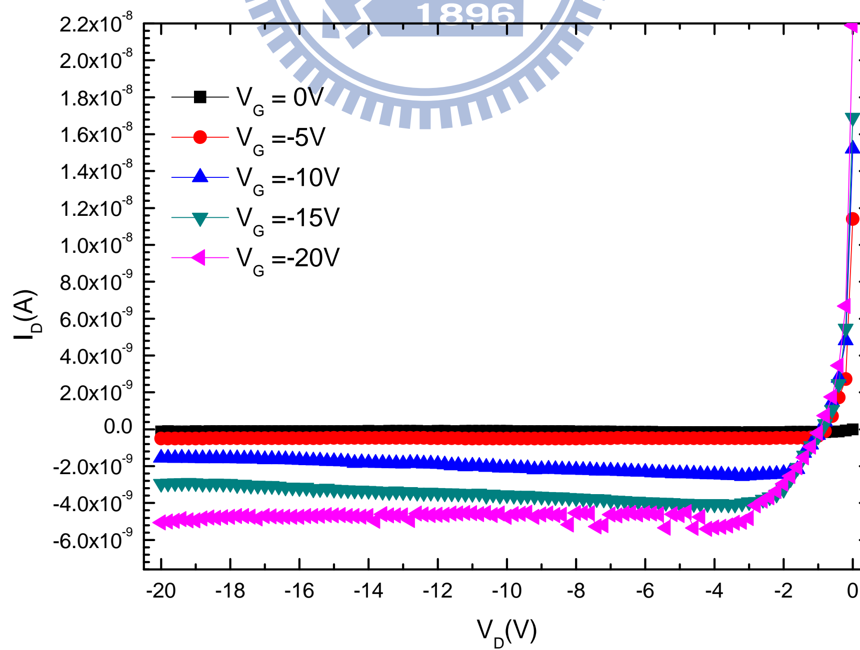


(b)

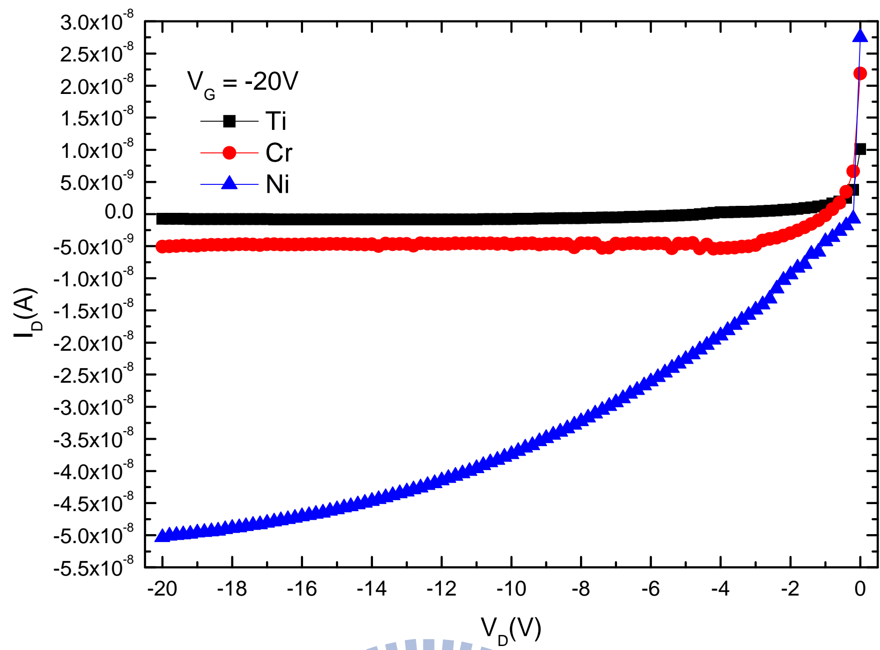


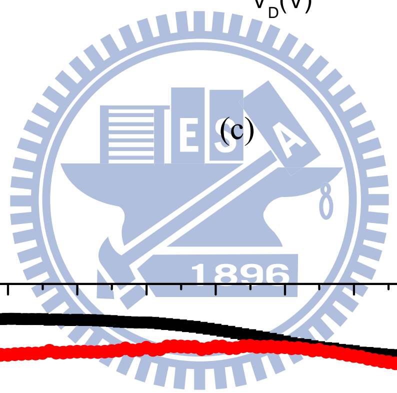

(c)

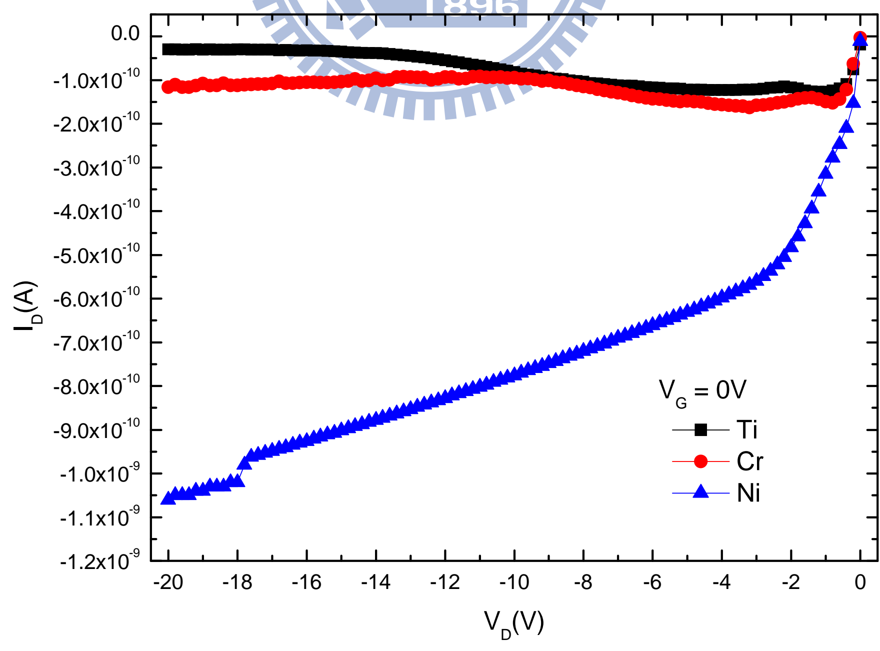


(d)

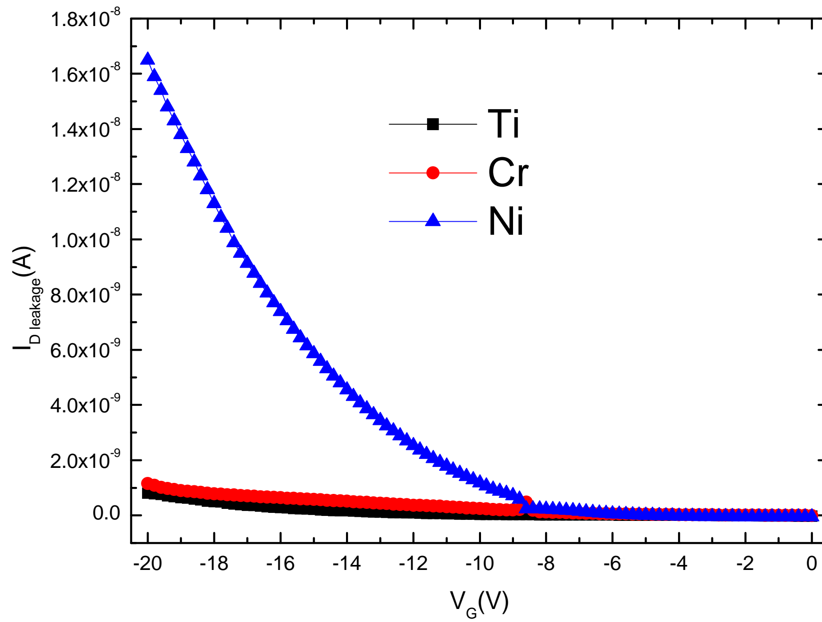


(e)

Figure 3-12 The output characteristic curves of OTFTs which consist of (a) Ti electrode, (b) Cr electrode, (c) comparison of $V_G = 20V$, (d) comparison of $V_G = 0V$, (e) comparison of $I_{D\ leakage}$.

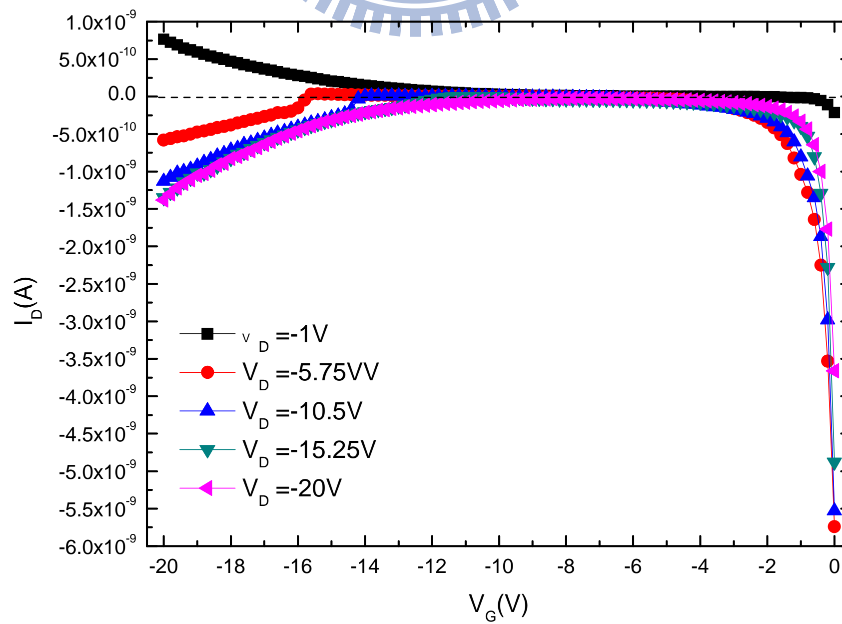


(a)

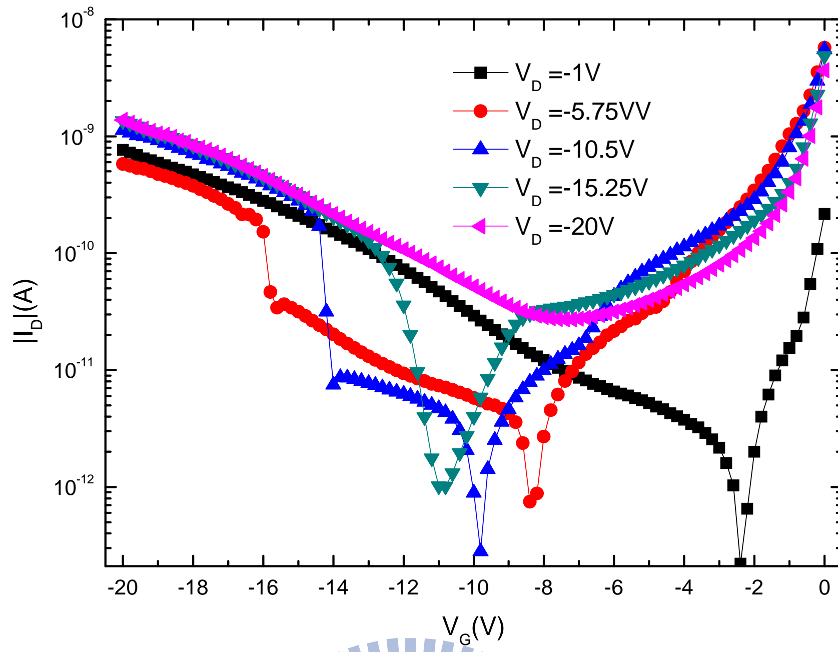


(b)

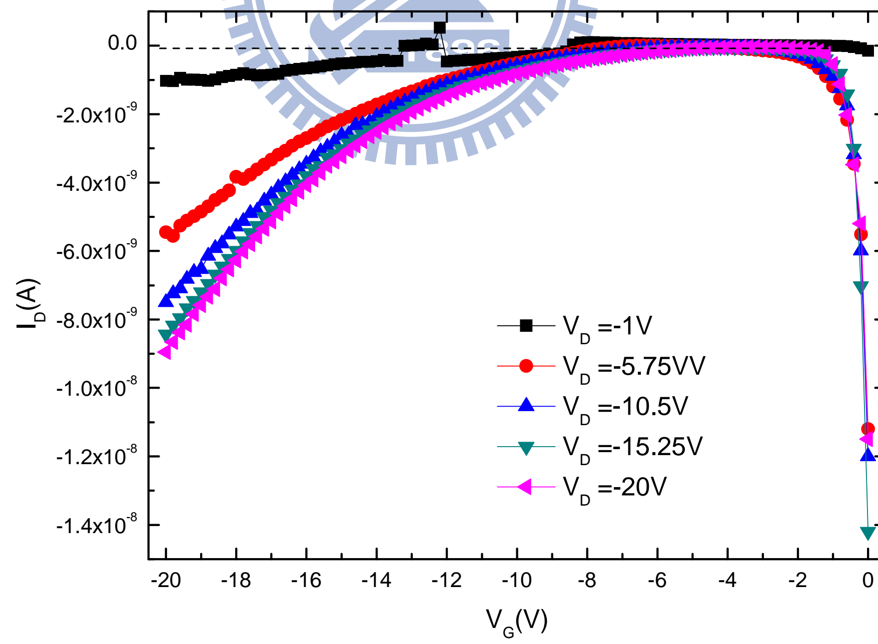


(c)

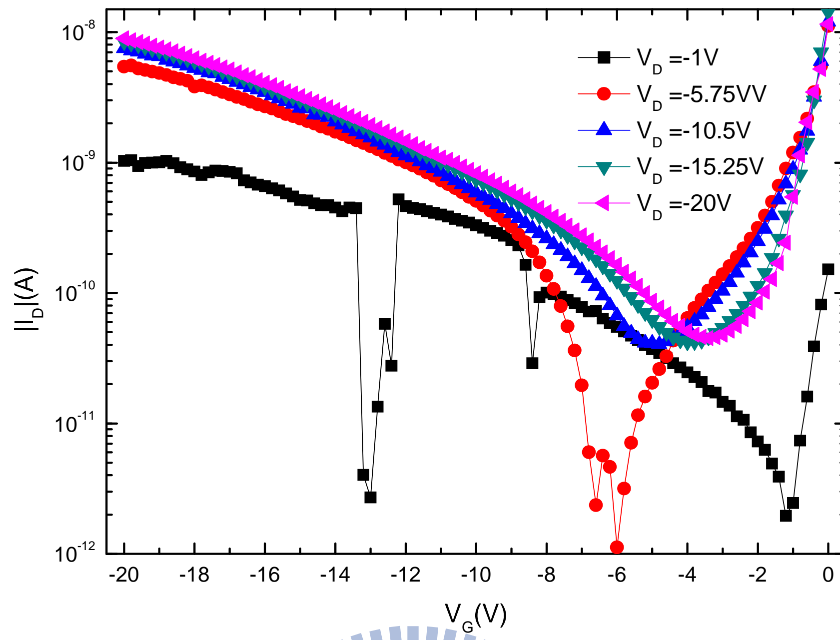


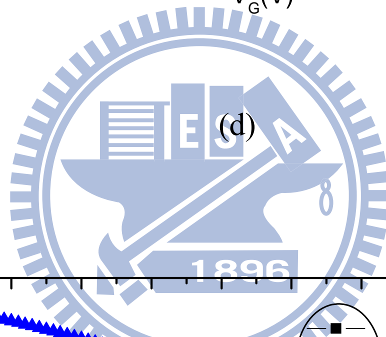
(d)

(d)

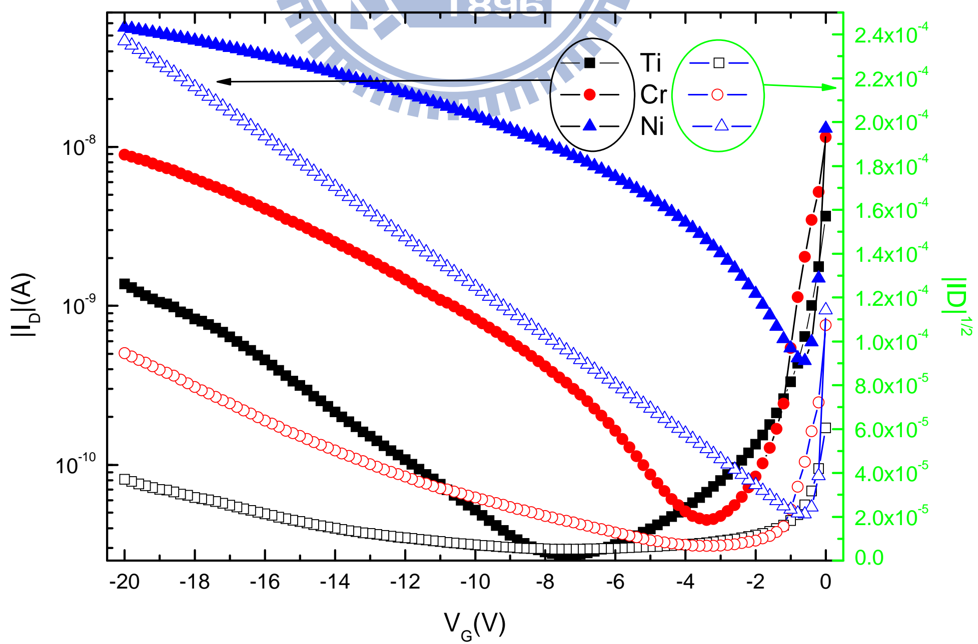


(e)

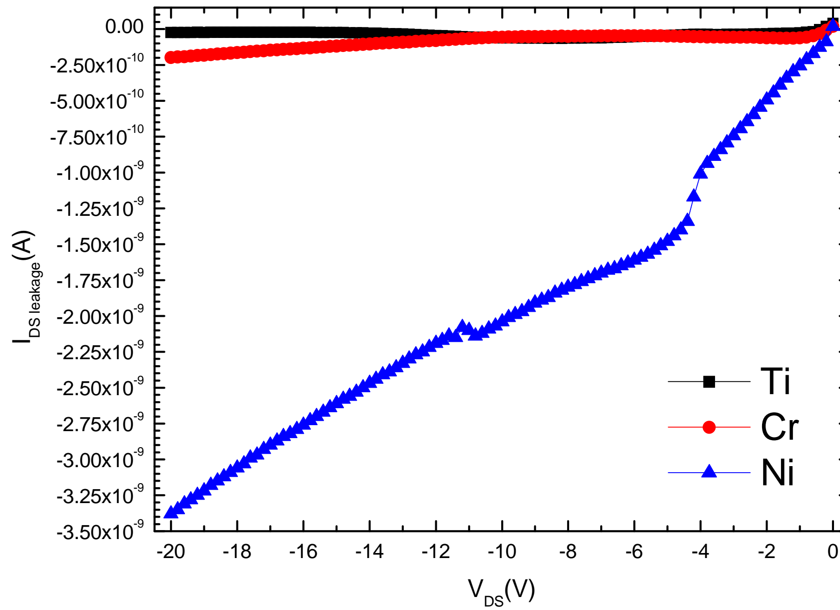


(f)

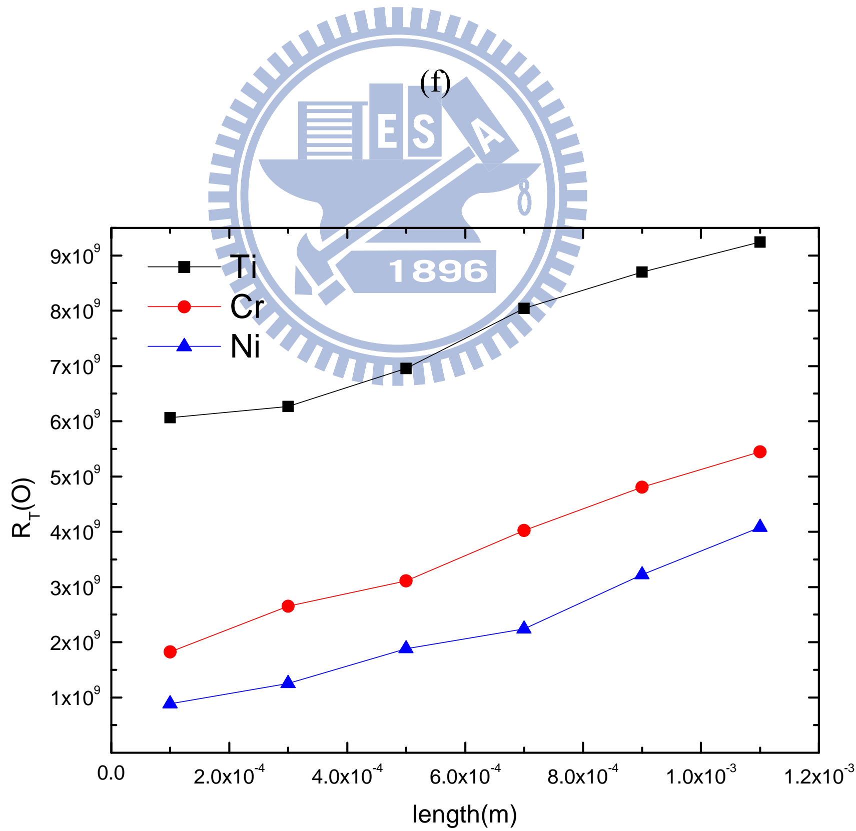


(g)

Figure 3-13 The transfer characteristic curves of OTFTs which consist of (a) Ti electrode, (b) $|I_D|$-$V_G$ curves of Ti electrode, (c) Cr electrode, (d) $|I_D|$-$V_G$ curves of Cr electrode, (e) comparison of $V_D$ = -20V, (f) comparison of $I_{DS\ leakage}$, (g) comparison of total resistance ($R_T$) versus the length.

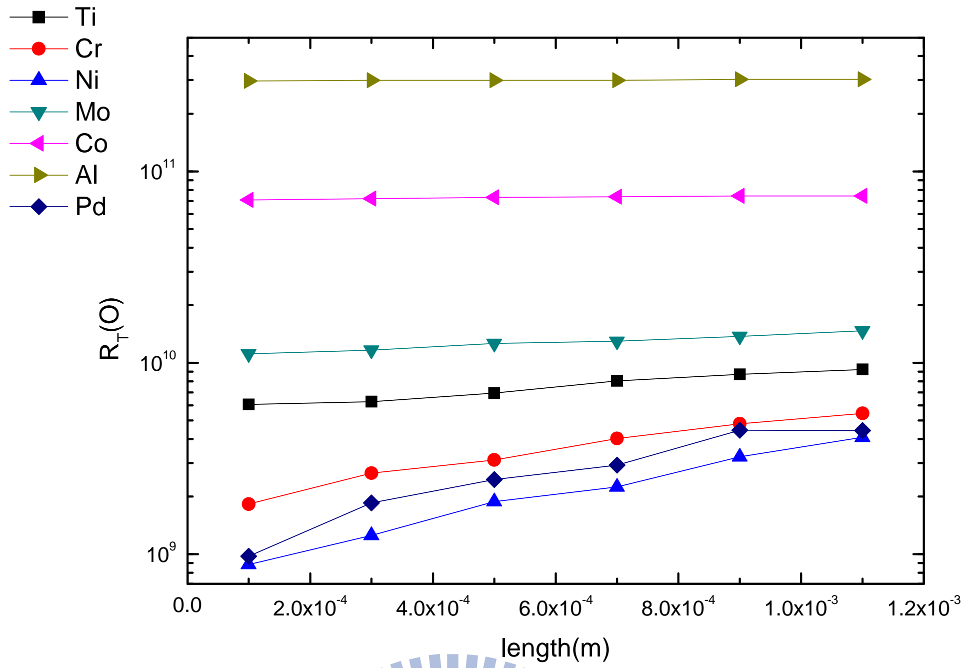


(a)

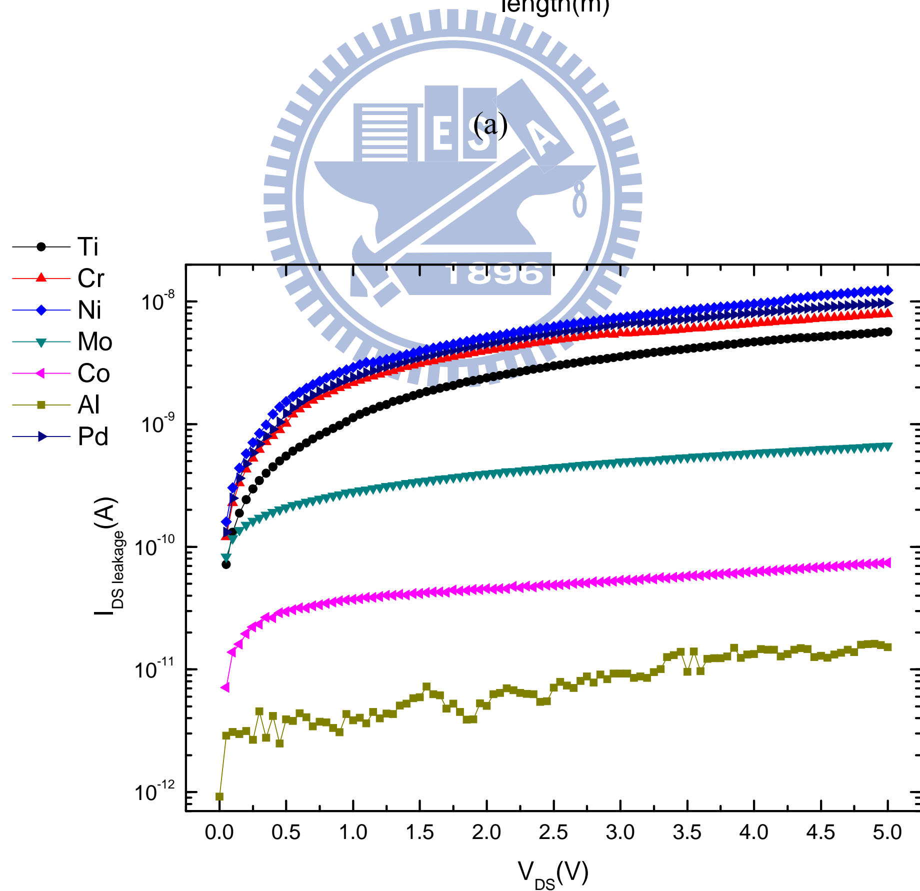


(b)

Figure 3-14 The curves consist of (a) comparison of total resistance ($R_T$) versus the length and (b) $I_{DS\ leakage}$ with all metals.

Table 3-1 The parameter of all metals which measured with the transfer length method.

| | Al | Ti | Cr | Mo | Co | Pd | Ni |
|---|---|---|---|---|---|---|---|
| $\varphi_m$(eV) | 4.28 | 4.33 | 4.5 | 4.6 | 5 | 5.12 | 5.15 |
| $R_s$(Ω/square) | 0.89E10 | 0694E10 | 0.728E10 | 0.692E10 | 0.732E10 | 0.728E10 | 0.636E10 |
| $R_C$(GΩ) | 148 | 2.7 | 0.73 | 5.4 | 35.5 | 0.033 | 0.018 |
| Boiling point | 2467 | 3287 | 2672 | 4612 | 2870 | 2927 | 2732 |
| $\chi$ | 1.61 | 1.54 | 1.66 | 2.16 | 1.88 | 2.2 | 1.91 |

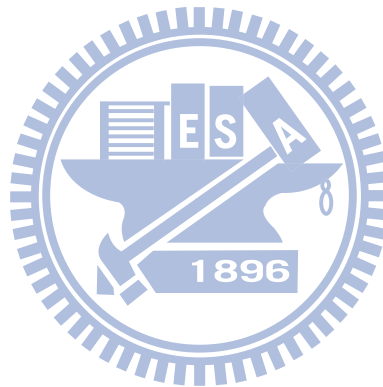

# Chapter 4 Conclusion and Future work

## 4.1 Conclusion

In this study, we rigorously analyzed the origin which caused the distortion of performance curve, and we comprehended that the $I_{D\ leakage}$ and $I_{DS\ leakage}$ is the main contribution that cause the distortion of performance curve. Additionally, patterning the organic active layer will greatly reduce the $I_{G\ leakage}$. Accordingly, the $I_{D\ leakage}$ will be decreased, too.

Surface treatment on gate insulator can improve the mobility of OTFTs and even reduce the threshold voltage because the order of organic material got better. However,$I_{G\ leakage}$ and $I_{DS\ leakage}$ are also increased with the improvement of the order of organic material.

Reducing the hole-injection barrier with metals have higher work function may predict in certain of material, yet the increase on $I_{D\ leakage}$ and $I_{DS\ leakage}$ is the inevitable supplementary impact.

We comprehend that interface properties can't be predicted solely on work function and IP. Additionally, comparing to BC, the parameters (e.g., depositing rate, pressure, surface morphology of semiconductor, boiling point of metals etc.) during the depositing of metal atoms may also have influence on interface properties. But our measurement of contact resistance exactly predicted the on-current and leakage (Fig. 3-14). That is, the transfer length method may be used to predict whether the metals suit to be electrode.

## 4.2 Future work

As mention above, the origin which distort the electric characteristics of OTFTs are $I_{G\ leakage}$ and $I_{DS\ leakage}$. A high quality gate insulator fabricated with low temperature processes is urgent for OTFTs to reduce power consumption and to suppress the $I_{G\ leakage}$. However, when scaling down to the channel length, the anomalous leakage current ($I_{DS\ leakage}$) will becomes conspicuous. In order to obtain the suppression of $I_{DS\ leakage}$, the p/n junction-like structure of traditional MOFET may be a useful notion that used in fabrication of organic active layer.

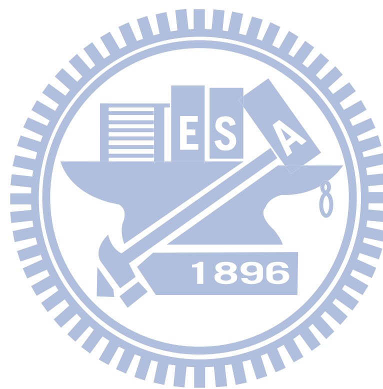

# References

[1] F. J. Mayer zu Heringdorf, M. C. Reuter, and R. M. Tromp, Nature, Volume 412, August 2001, Pages 517-520.

[2] C. D. Dimitrakopoulos, and D. J. Mascaro, “Organic thin-film transistors: A review of recent advances”, Volume 45, Issue 1, January 2001, Pages 11-27.

[3] A. R. Brown, C. P. Jarrett, D. M. de Leeuw, and M. Matters, “Field-effect transistors made from solution-processed organic semiconductors”, Synthetic Metals, Volume 88, Issue 1, April 1997, Pages 37-55.

[4] Tony Blythe, and David Bloor, Electrical Properties of Polymers, UK: Cambridge, 2005, Pages 111-153.

[5] Sang Yoon Yang, Kwonwoo Shin, and Chan Eon Park, “The Effect of Gate-Dielectric Surface Energy on Pentacene Morphology and Organic Field-Effect Transistor Characteristics”, Advanced Functional Materials, Volume 15, Issue 11, September 2005, Pages 1806-1814.

[6] Marcus Ahles, Roland Schmechel, and Heinz von Seggern, “n-type organic field-effect transistor based on interface-doped pentacene”, Applied Physics Letters, Volume 85, Issue 19, November 2004, Pages 4499-4501.

[7] F. A. Yildirim, R. R. Schliewe, W. Bauhofer, R. M. Meixner, H. Goebel, and W. Krautschneider, “Gate insulators and interface effects in organic thin-film transistors”, Organic Electronics, Volume 9, Issue 1, February 2007, Pages 70-76.

[8] Janos Veres, Simon Ogier, and Gilles LloydDago de Leeuw, “Gate insulators in Organic Field-Effect Transistors”, Chemistry of Materials, Volume 16, Issue 23, September 2004, Pages 4543-4555.

[9] Dimas G. de Oteyza, Esther Barrena, J. Oriol Osso, Helmut Dosch, Stephan Meyer, and Jens Pflaum, “Controlled enhancement of the electron field-effect mobility of $F_{16}CuPc$ thin-film transistors by use of functionalized $SiO_2$ substrates”, Applied Physics Letter, Volume 87,Issue 18, October 2005, Pages 183504.

[10] Iwao Yagi, Kazuhito Tsukagoshi, and Yoshinobu Aoyagi, "Modification of the electric conduction at the pentacene/$SiO_2$ interface by surface termination of $SiO_2$", Applied Physics Letter, Volume 86, Issue 10, February 2005, Pages 103502.

[11] S. Kobayashi, T. Nishikawa, T. Takenobu, S. Mori, T. Shimoda, T. Mitani, H. Shimotani, N. Yoshimoto, S. Ogawa, and Y. Iwasa, "Control of carrier density by self-assembled monolayers in organic field-effect transistors", Nature Materials, Volume 3, May 2004, Pages 317-322.

[12] P. Too, S. Ahmed, B. J. Sealy, and R. Gwilliam, "Electrical characterization of Fe-doped semi-insulating InP after helium bombardment at different implant temperatures", Applied Physics Letters, Volume 80, Issue 20, May 2002, Pages 3745-3747.

[13] Han Jin Ahn, Soon Joon Rho, Kyung Chan KIM, Jong Bok Kim, Byoung Har Hwang, Chang Joon Park, and Hong Koo Baik, "Ion-Beam Induced Liquid Crystal Alignment on Diamond-like Carbon and Fluorinated Diamond-like Carbon Thin Films", Japanese Journal of Applied Physics, Volume 44, June 2005, Pages 4092-4097.

[14] Gilles Horowitz, "Organic thin film transistors: From the theory to real devices", Materials Research Society, Volume 19, Issue 7, July 2004, Pages1946-1962.

[15] Sung Hun Jin, Keum Dong Jung, Hyungcheol Shin, Byung-Gook Park, and Jong Duk Lee, "Grain size effect on contact resistance of top-contact pentacene TFTs", Synthetic Metals, Volume 156, January 2006, Pages 196-201.

[16] Dong-Jin Yun, Sang-Hoon Lim, Seung-Hwan Cho, Bo-Sung Kim, and Shi-Woo Rhee, "Effect of Cu, CuO, and Cu-CuO Bilayer Source/Drain Electrodes on the Performance of the Penctacene Thin-Film Transistor," Journal of Electrochemical Society, Volume 156, Issue 8, June 2009, Pages H634-H639.

[17] Hsiao-Wen Zan and Cheng-Wei Chou, "Effect of Surface Energy on Pentacene Thin-Film Growth and Organic Thin Film Transistor Characteristics," Japanese Journal of Applied Physics, Volume 48, March 2009, Pages 031501.

[18] D. J. Gundlach, L. Zhou, J. A. Nichols, T. N. Jackson, P.V. Necliudov and M. S. Shur, "An experimental study of contact effects in organic thin film transistors", Journal of Applied Physics, Volume 100, Issue 2, July 2006, Pages 024509.

[ 19]P. G. Schroeder, C. B. France, J. B. Park and B. A. Parkinson, "Orbital Alignment and Morphology of Pentacene Deposited on Au(111) and SnS2 Studied Using Photoemission Spectroscopy", The Journal of Physical Chemistry, February 2003, Volume 107, Issue 10, February 2003, Pages 2253-2261.

[20] K. S. Lee, T. J. Smith, K. C. Dickey, J. E. Yoo, K.J. Stevenson and Y. L. Loo, "High-Resolution Characterization of Pentacene/Polyaniline Interfaces in Thin-Film Transistors", Advanced Functional Materials, Volume16, Issue18, Pages 2409-2414.

[ 21] Dipti Gupta, M. Katiyar, and Deepak Gupta, "An analysis of the difference in behavior of top and bottom contact organic thin film transistors using device simulation", Organic Electronics, Volume 10, Issue 5, August 2009, Pages 775-784.

[22] H. E. Katz, W. Li, A. J. Lovinger, J. Laquindanum, "Solution-phase deposition of oligomeric TFT semiconductors", Synthetic metals, Volume 102, Issues 1-3, June 1999, Pages 897-899.

[23] Shuo-Cheng Wang, Jen-Chung Lou, Bo-Lin Liou, Ron-Xion Lin, and Ching-Fa Yeh, "Process Improvement and Reliability Characteristics of Spin-On Poly-3-hexylthiophene Thin-Film Transistor", Journal of The Electrochemical Society, Volume 152, Issue 1, 2005, Pages G50-G56M.

[24 ] Slimane Oussalah, Boualem Djezzar, and Robert Jerisian, "A comparative study of different contact resistance test structure dedicated to the power process technology", Solid-State Electronics, Volume 49, Issue 10, October 2005, Pages 1617-1622.

[25] Dong-Jin Yun, Dong-Kyu Lee, Hwan-Ki Jeon and Shi-Woo Rhee, "Contact resistance between pentacene and indium-tin oxide(ITO) electrode with surface treatment", Organic Electronics, Volume 8, Issue 6, December 2007, Pages 690-694.

[26]Dieter K., and Schroder, Semiconductor Material and Device Characterization, New Jersey: Wiley-Interscience, 2006, Pages 135-149.

[27] A. Salleo, M. L. Chabinyc, M. S. Yang, and R. A. Street, “Polymer thin-film transistors with chemically modified dielectric interfaces”, Applied Physics Letters, Volume 81, Issue 23, November 2002, Pages 4383-4385.

[28] T. C. Gorjanc, I. Levesque, and M. D’lorio, “Organic field effect transistors based on modified oligo-*p*-phenylevinylenes”, Volume 84, Issue 6, February 2004, Pages 930-932.

[29] Chin-Hsian Lin, Enhancing the properties of polymer thin-film transistors using a novel atmospheric-pressure plasma technology, Ph. D. Thesis, National Chiao Tung University, Taiwan, 2008.

[30] Shi-Woo, Rhee, and Dong-Jin Yun, “Metal-Semiconductor contact in organic thin film transistors,” Journal of Materials Chemistry, Volume 18, Issue 45, 2008, Pages 5437-5444.

[31] Peter V. Necliudov, Michael S. Shur, David J. Gundlach, and Thomas N. Jackson, “Contact resistance extraction in pentacene thin film transistors,” Solid-State Electronics, Volume 47, Issue 2, February 2003, Pages 259-262.

[32] Jana Zaumseil, Richard H. Friend, and Henning Sirringhaus, “Spatial control of the recombination zone in an ambipolar light-emitting organic transistor,” Nature Materials, Volume 5, December 2005, Pages 69-74.